Hydraulics Research
Wallingford

The Nearshore Profile Model

Further Model Development and Sensitivity Tests

H N Southgate MA, PhD

Report SR 234
March 1990

Registered Office: Hydraulics Research Limited, Wallingford, Oxfordshire OX10 8BA.
Telephone: 0491 35381. Telex: 848552

This report describes work carried out by Hydraulics Research under Commission 14D1 funded by the Ministry of Agriculture, Fisheries and Food, nominated officer Mr A J Allison. At the time of reporting this project, Hydraulics Research's nominated project officer was Dr S W Huntington.

This report is published on behalf of the Ministry of Agriculture, Fisheries and Food, but any opinions expressed are those of the author only, and not necessarily those of the ministry.

ABSTRACT

This report describes modifications and improvements to the Nearshore Profile Model developed at Hydraulics Research for predicting detailed nearshore wave, current and sediment transport processes. These improvements are to the representation of wave energy dissipation by bottom friction and, principally, wave breaking. An accurate representation of these processes is crucial to the whole model since breaking waves in particular provide the most important driving forces for surf zone processes. A range of validation and sensitivity tests incorporating these model improvements is described. Work described in this report is complementary to extensive further development of the Nearshore Profile Model carried out jointly by Hydraulics Research and the Department of Civil Engineering at Imperial College, London for Sir William Halcrow and Partners (Report EX 2010, availability subject to the permission of the collaborating institutions).

CONTENTS

CONTENTS (CONT'D)

FIGURES

1. INTRODUCTION

This report describes modifications and improvements to the computational modelling of the dissipative processes of seabed friction and wave breaking, on the propagation of waves in shallow water. This work has been carried out using HR's Nearshore Profile Model (NPM), and the techniques should be suitable for other types of shallow-water wave transformation model.

The NPM is designed to model in detail the transformation of waves in nearshore regions and, in particular, in the surf zone where wave breaking is the dominant process and provides the driving forces for other surf zone processes. The NPM assumes a straight coastline with parallel depth contours and determines wave and longshore current parameters at grid points along a shore-normal profile line (see Fig 1). The theory of the NPM, its computational techniques and some comparisons with laboratory and field data are described in Southgate (1988 and 1989). A copy of the latter paper is reproduced in the Appendix, and references to equations in the Appendix will be made from the main text of this report.

Recently, improvements have been made to the representations of bottom friction and, particularly, wave breaking. Validation tests using this new version of the model have been made against field measurements from the Nearshore Sediment Transport Study (NSTS) Experiment at Leadbetter Beach, Santa Barbara, California conducted during January and February 1980. A series of further tests have been carried out to assess the sensitivity of predicted surf zone parameters to the model improvements and empirical input data.

Chapters 2 and 3 describe the Leadbetter Beach measurements and the results of the comparison between these and the NPM predictions. Chapter 4 describes the improvements to the modelling of wave energy dissipation, and the results of the sensitivity tests. A summary of the work is given in Chapter 5.

2. COMPARISON OF NPM PREDICTIONS AND LEADBETTER BEACH MEASUREMENTS

The model has been verified against a comprehensive field data set from the Nearshore Sediment Transport Study (NSTS) Experiment at Leadbetter Beach, Santa Barbara, California, conducted during January and February 1980. This exercise included detailed wave, current and sediment movement measurements in and near the surf zone at a site consisting of a long straight beach with approximately parallel depth contours, thus largely satisfying the longshore homogeneity requirement for the Nearshore Profile Model.

The instrumentation consisted of arrays of e/m current meters and wave pressure sensors situated along a profile line at varying distances from the waterline. Incident wave heights (rms values) were obtained from a pressure sensor in about 4m depth of water at high tide (about 80m from the waterline). Incident wave directions were obtained from directional wave measurements in about 9m of water, modified to account for refraction to the 4m contour. The comparisons presented in this report are for measurements made during the five-day period from February 2 to February 6, 1980, during which the wave conditions were reasonably narrow-banded in frequency and direction. On each of these days, the beach profile was measured and one set of wave and current

measurements was made at high tide. The tidal range was small, less than 2m, and tidal currents were ignored in the analysis of the field data. Details of the field measurements and the derived data are given in Thornton and Guza (1986). Further details of the NSTS program and the Leadbetter Beach study may be found in Gable (1981) and Seymour (1987).

3. RESULTS OF THE VALIDATION TESTS

The seabed profiles for each day were digitised into a grid consisting of 110 nodes with the following spacings:

Distance from Offshore Point (m)	Number of Grid Intervals	Width of Grid Intervals (m)
0 - 47.5	19	2.5
47.5 - 92.5	90	0.5

The distance from the offshore point to the waterline was 80m; some dry grid points are therefore included beyond the waterline.

Input data to the computational model consisted of the incident wave period, angle, and rms wave height. Average values of the ratio of breaking wave height to depth in the surf zone were determined during the field data analysis for each day's measurements, and were supplied to the model as input parameters for use in the breaking criterion of Weggel (1972) (see Equations 12-14 in the Appendix). These values were adjusted slightly to give a best fit (judged by eye) between the computed and measured distributions of rms wave height and longshore current velocity. In addition, the following constant data were used, a

sediment size of 200 microns, a seabed roughness height of 0.016m (a typical value for this size of sediment), and an acceleration due to gravity of $9.81 ms^{-2}$. The maximum number of iterations between the wave and current modules was set at four, a value which was found to give convergence of all wave and current parameters.

The input data for the verification tests is summarised in Table 1. These are 'standard' data, designed to give a best fit to the field measurements. Comparisons of predicted and measured rms wave heights and longshore wave-induced current velocities are shown in Figures 2-6. The results are quite satisfactory, bearing in mind the simplifications in the representation of surf zone physical processes which have been made in the model (see Appendix). The main purpose of the work in this report is to test the sensitivity of model predictions to the values of various input parameters.

4. SENSITIVITY OF MODEL PREDICTIONS

The Nearshore Profile Model contains a number of input parameters for which empirically determined values need to be specified. Ideally the model would be calibrated against measured data for a particular site, but very often such data is not available or suitable. In such circumstances, these values should be based on previous uses of the model at sites with similar wave and tidal conditions. An essential part of making this choice is an understanding of what the effect of variations in the values of the input parameters has on the final predictions (usually of rms wave height and longshore current velocity). In this chapter a series of tests are carried out in which the values of the input parameters for the

February 5 Leadbetter Beach data set (see Table 1 and Fig 5) are varied, in order to indicate the sensitivity of results to these input parameters.

4.1 The breaker constant, a', in the modified Weggel breaker criterion

The model contains the option of using one of two wave breaker height criteria, those due to Weggel (1972) as modified according to Southgate (1989) (see Appendix), and Battjes and Stive (1985). Of these two criteria, only Weggel requires an empirically-determined input parameter. This criterion is based on a large set of laboratory data using monochromatic waves. The extension to its use for random waves is therefore somewhat debatable, but is overcome to some extent by the flexibility in the choice of a'. The verification tests against monochromatic-wave laboratory data (described in the Appendix), both indicate good agreement in rms wave height and longshore current velocities with a suitable choice of a'.

Typical values of a' are around 0.78 (the value in the original Weggel criterion) but considerably smaller values (around 0.40) have been used in the Leadbetter Beach tests. The choice of this parameter has quite a marked effect on model results, and it is therefore important to choose the value carefully and to understand its effect on predicted wave heights and longshore current velocities. The overall effect is that larger values of a' cause waves to break closer to the shore, resulting in a larger wave height at the breaker point, a narrower surf zone, and a steeper wave height decay in the surf zone. The effect on longshore current velocity is to cause a higher peak,

closer inshore, and a steeper decay to both landward and seaward.

Figure 7 shows a plot of rms wave height with the original value of a' = 0.38, and with new values of a' = 0.33 and 0.43. Figure 8 shows a similar comparison for longshore current velocities. These figures bear out the description of the effects of the variation of a' on the overall predictions (see previous paragraph). They also indicate that the results are quite sensitive to the value of a'. This value has to be chosen carefully since it will vary significantly from site to site and according to the type of incident wave conditions. Generally lower values are used for low steepness (swell) waves, as at Leadbetter Beach, and higher values for high steepness (wind sea) waves, typical of many UK coastal sites.

4.2 Comparison of breaker criteria of Weggel (1972) and Battjes and Stive (1985)

The model contains the option of using the breaker criterion due to Weggel (1972) or Battjes and Stive (1985). The Battjes criterion is based on curve fitting to a number of laboratory and field measurements with random waves. Somewhat surprisingly, Battjes and Stive found no systematic dependence on seabed slope, but a weak dependence on offshore steepness. An empirical fit using a tanh function was made to the data:

$$(H/h)_b = 0.5 + 0.4 \tanh (33\ s_o) \qquad (1)$$

where $(H/h)_b$ is the ratio of rms wave height to water

depth at breaking in shallow water, and s_o is the deep-water wave steepness. In the comparison with the Leadbetter Beach data, this formula has been found to give values of $(H/h)_b$ which are too high (see Fig 9). Accordingly the data used by Battjes and Stive have been re-analysed (R B Nairn, private communication), including the Leadbetter Beach data set, and a new best-fit criterion made:

$$(H/h)_b = 0.39 + 0.56 \tanh (33\ s_o) \qquad (2)$$

This improves the model predictions for Leadbetter Beach. Figures 9 and 10 show the rms wave height and longshore current velocities using Equations 1 and 2, and the Weggel criterion with the best-fit value of $a' = 0.38$. It can be seen that the new Battjes criterion (Eq 2) gives wave height results of the same accuracy as Weggel, but the original Battjes criterion tends to over-predict wave heights in the surf zone. Comparing longshore current velocities, there is similar agreement between Weggel and new Battjes, with old Battjes predicting a general landward shift. The Battjes criterion has the advantage over Weggel of not requiring specification of an input parameter, but for the same reason is liable to be less accurate at uncalibrated sites, bearing in mind the different values of $(H/h)_b$ at different sites. As experience of using the model increases, it would be valuable to include additional random-wave data sets to provide a more accurate and widely applicable expression of the Battjes type.

4.3 Rate of wave energy dissipation inside the surf zone

As a wave travels into shallow water, there comes a point where the rms wave height (H_{rms}) exceeds the local value of the breaker height (H_b). When this occurs, most models using the Battjes and Janssen (1978) wave breaking method (based on a tidal bore analogy) truncate H_{rms} to be equal to the local value of H_b. The same truncation takes place at shallower depths where H_{rms} exceeds the local value of H_b. In the present model H_{rms} is truncated in the same way, but the energy dissipated in the broken wave is still calculated according to the tidal bore analogy (see Eqs 17-19 in the Appendix). This is denoted as Method A. This method is in contrast to some other models (eg Thornton and Guza (1986)) where the tidal bore formula is abandoned in this region, and the dissipated broken wave energy is calculated directly from the local truncated values of H_{rms} (Method B).

Figure 11 shows the longshore current velocities using the two methods. It can be seen that a very irregular longshore current profile is obtained using Method B. This irregular appearance is due to the strong dependence of the wave radiation stress driving forces on H_{rms}, which in turn is strongly dependent on the water depth. Any departure from a regular depth profile will tend to be magnified in the calculation of the longshore current velocity distribution. It is possible that with a perfectly straight slope, or with some smoothing process, a more regular shape could be

obtained, but the agreement with the Leadbetter Beach data would still be considerably poorer.

Apart from the better model predictions, there are some plausible physical reasons for the retention of the tidal bore method in the inner surf zone. The fact that not all the reduction in wave height is accounted for by the turbulent dissipation of broken wave energy implies that some of the wave energy is converted into some other type of ordered water motion on the scale of (at least) a wavelength. This could be in the form of uni-directional water motion in the direction of wave travel which would provide the momentum for wave run-up on a beach once the broken wave has died away. Another possibility is the conversion of primary wave energy into long waves. Recent experience has shown that a significant proportion of primary wave energy can be converted to long waves trapped close to the coastline.

4.4 Asymptotic behaviour of wave energy dissipation rate at the shoreline

It has been found that, under certain circumstances, the model predicts that the rate of wave energy dissipation rises strongly very close to the shoreline, causing a sharp peak in predicted longshore current velocity. Figure 12 shows this effect. It has been necessary therefore to modify the wave energy dissipation formula to give the correct asymptotic behaviour very close to the waterline. This is done in the following way. The water depth (h_c) at which the rms wave height first exceeds the local breaker height is noted. The rms wave height is subsequently truncated to the local breaker height but, as

explained in Section 4.3, the tidal bore formula is still used to calculate the wave energy dissipation rate. When the water depth falls below some pre-specified fraction (f_c) of h_c, the dissipation parameter (β in eq 25 of the Appendix) is fixed at that constant value as far as the waterline, unless the depth increases again to a value greater than h_c at which point the full expression for β is used again. This procedure is somewhat arbitrary but agrees well with the measured data at Leadbetter Beach, and is necessary to give the correct asymptotic behaviour at the waterline.

Trial runs revealed that a value of $f_c = 0.6$ gave the best agreement with the Leadbetter Beach data for each of the five days' data. Figure 12 shows the effect on the calculation of longshore current velocity of setting f_c equal to 0.6, 1.0 (corresponding to using a constant value of β immediately when H_{rms} first exceeds H_b) and 0 (corresponding to using the full expression for β everywhere). It can be seen that $f_c = 0$ gives a sharp peak in longshore current velocity very close to the waterline, while $f_c = 1$ underpredicts values in the surf zone.

4.5 The tidal bore expression for broken wave energy dissipation

In the expression for energy dissipation for broken waves (Eq 18 in the Appendix), there is a parameter, λ, whose purpose is to account for the differences between the tidal bore and broken wave processes. A

good fit to each of the Leadbetter Beach data sets has been obtained with a value of $\lambda = 1$ (ie no difference between the two processes). Figures 13 and 14 show the effects of varying λ slightly to 0.8 and 1.2, and a much larger variation to 5.0 (a value which has been used in other validation tests, see Hydraulics Research Report EX 2010). These figures show that rms wave heights around the breaker point decrease slightly with increasing λ for values between 0.8 and 1.2, and show a larger jump for $\lambda = 5.0$. Results for the longhsore current velocities indicate a noticeable λ dependence for values of 0.8 and 1.2, and a very significant change for $\lambda = 5.0$.

4.6 Seabed roughness height

The NPM contains the option of using a constant pre-specified seabed roughness height, k_s, at all grid points, or of using a formula due to Swart (see Sleath (1984), p40) relating the roughness height to the local seabed ripple height and length. In the comparison with the Leadbetter Beach data, a constant roughness height of 0.016m (a typical value for fine to medium sand) was used in all the tests. Figures 15 and 16 show the effects of using different values of k_s, of 0.008m and 0.024m. The effect on rms wave height is negligible, expressing the fact that the wave friction factor is only weakly dependent on k_s and that frictional dissipation of wave energy is much smaller over short distances in the surf zone than dissipation by breaking. The effect on longshore currents is, however, quite noticeable.

Further tests were carried out using the Swart formula for k_s instead of the constant pre-specified value. Figures 17 and 18 show that there is again a negligible effect on rms wave height, but

significantly higher longshore current velocities are predicted. This is the result of the rapid spatial changes of k_s predicted by the Swart formula. At the offshore point a value of about 0.04m is predicted; this decreases by a factor of about 20 before regaining a value of about 0.03m very close to the waterline. This demonstrates a high sensitivity of k_s to the ripple dimensions. These dimensions themselves are of dubious accuracy, since seabed ripples are influenced by the local current field and by previous strong wave events as well as by the present wave conditions. A suitably chosen constant value of k_s is therefore recommended.

5. SUMMARY AND CONCLUSIONS

This report describes various improvements to HR's Nearshore Profile Model in the representation of wave energy dissipation in the surf zone. Comparisons of model predictions against measured data recorded at Leadbetter Beach, California are made, with particular emphasis on the sensitivity of predictions to variations in a number of model parameters. These parameters are:

1. The breaker constant in the modified Weggel breaker criterion.
2. A comparison of the breaker criteria of Weggel (1972) and Battjes and Stive (1985).
3. Two methods of predicting the rate of wave energy dissipation inside the surf zone.
4. An empirical parameter controlling the asymptotic behaviour of wave energy dissipation rate at the shoreline.
5. An empirical parameter in the tidal bore expression for the dissipation of broken wave energy.
6. The seabed roughness height.

Recommendations about choices of values of these parameters are made.

6. ACKNOWLEDGEMENTS

D G Goldberg is thanked for his help with model runs and preparation of results. R B Nairn of Imperial College has contributed extensively to the further development of the model (Report EX 2010).

7. REFERENCES

1. Battjes J A and Janssen J P F M (1978), Energy Loss and Set-up due to Breaking of Random Waves, Proc 16th Int Conf on Coastal Eng, ASCE, Hamburg, pp569-587.

2. Battjes J A and Stive M J F (1985), Calibration and Verification of a Dissipation Model for Random Breaking Waves, J Geophys Res, Vol 90, No C5, pp9159-9167.

3. Gable C G (1981), Report on Data from the Nearshore Sediment Transport Study Experiments at Leadbetter Beach, Santa Barbara, California, IMR Ref No 80-5, Scripps Inst of Oceanography, La Jolla, California.

4. Hydraulics Research Ltd (1989), Nearshore Sediment Transport Model, Stage A, Report EX 2010.

5. Seymour R J (1987), An Assessment of NSTS, Proc Coastal Sediments '87, ASCE Speciality Conf, New Orleans, Vol 1, pp642-651.

6. Sleath J F A (1984), Seabed Mechanics, Pub, Wiley-Interscience.

7. Southgate H N (1988), The Nearshore Profile Model, Report SR 157, Hydraulics Research Ltd.

8. Southgate H N (1989), A Nearshore Profile Model of Wave and Tidal Current Interaction, Coastal Engineering, Vol 13, pp219-245.

9. Thornton E B and Guza R T (1986), Surf Zone Longshore Currents and Random Waves: Field Data and Models, J Phys Oceanography, Vol 16, No 7, pp1165-1178.

10. Weggel J R (1972), Maximum Breaker Height, J Waterways, Harbours and Coastal Div, ASCE, Vol 98, No WW4, pp529-548.

TABLE

	Date of Data Set				
	Feb 2	Feb 3	Feb 4	Feb 5	Feb 6
Depth at ~4m measurement point (m)	4.0	3.8	3.8	3.6	3.5
RMS wave height at ~4m measurement point (s)	0.40	0.55	0.56	0.45	0.26
Wave period at ~4m measurement point (s)	15.9	14.3	14.3	12.8	11.1
Wave direction at ~4m measurement point (°) (between profile line and forward ray direction)	6.4	7.8	9.0	8.4	8.3
Average bottom slope between shoreline and mean breaker line	0.059	0.044	0.038	0.035	0.033
Constant roughness height (m)	0.016	0.016	0.016	0.016	0.016
Breaking factor, λ, in tidal bore formula	1.0	1.0	1.0	1.0	1.0
Measured value of H/h in the surfzone	0.46	0.48	0.45	0.43	0.34
Breaking factor, a', used in Weggel breaker criterion	0.38	0.45	0.39	0.38	0.30
Observed breaker type	plunging	plunging	plunging	plunging/ spilling	plunging/ spilling

Table 1 Leadbetter Beach Validation Tests. Summary of Input Parameters.

FIGURES.

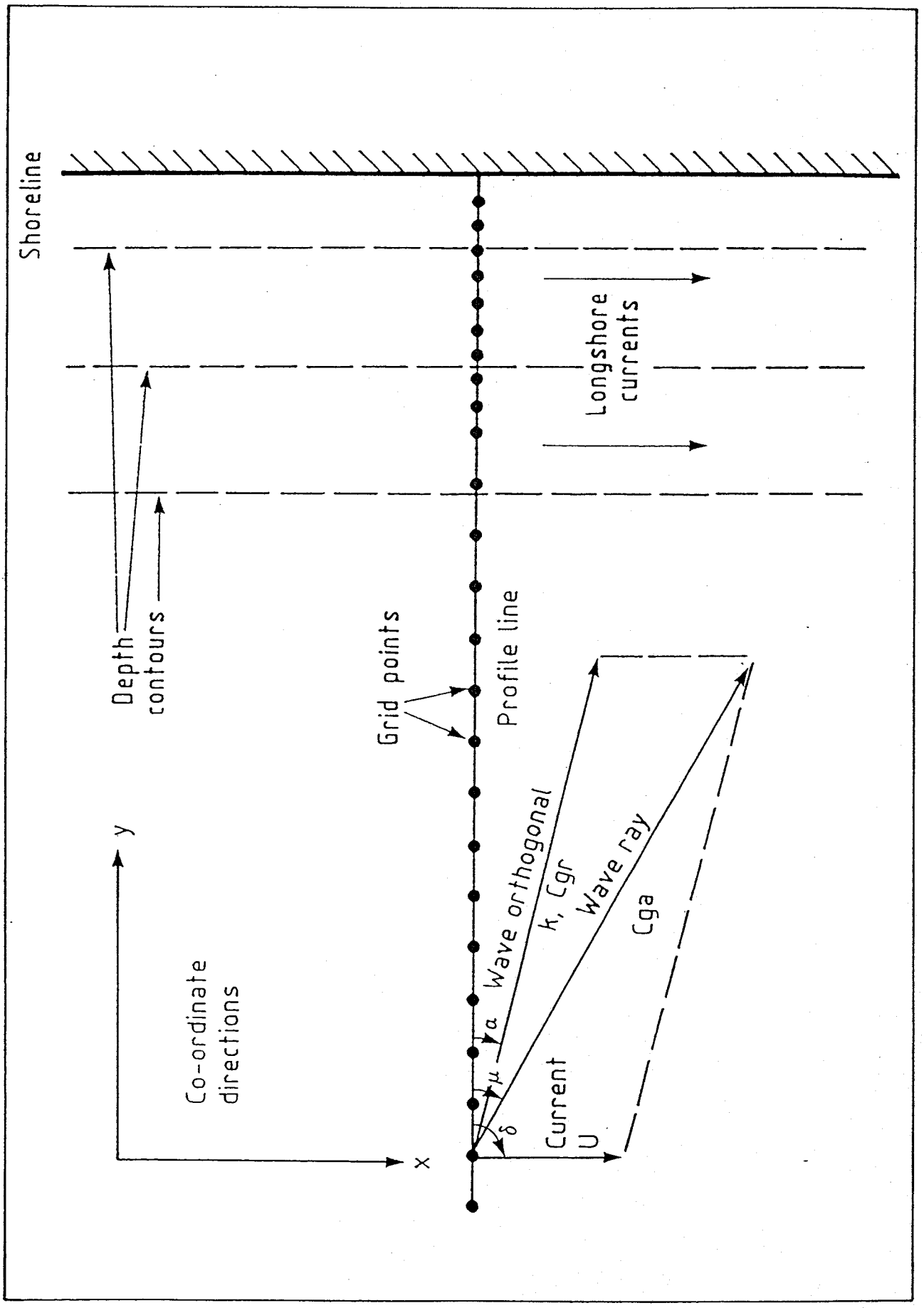

Fig 1 Model geometry of the Nearshore region

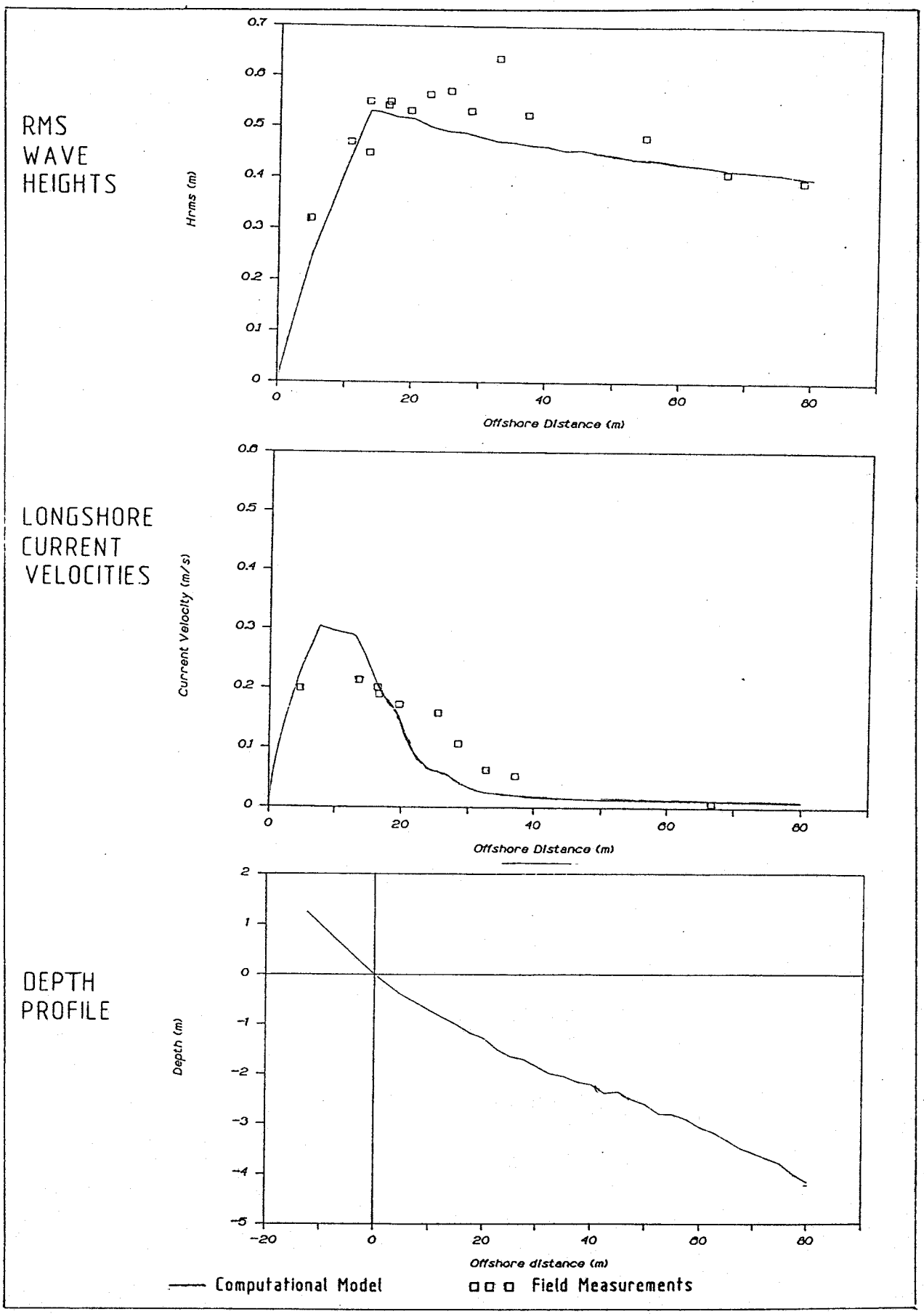

Fig 2 Comparison of Computational Model with Leadbetter Beach Data. Feb 2 1980

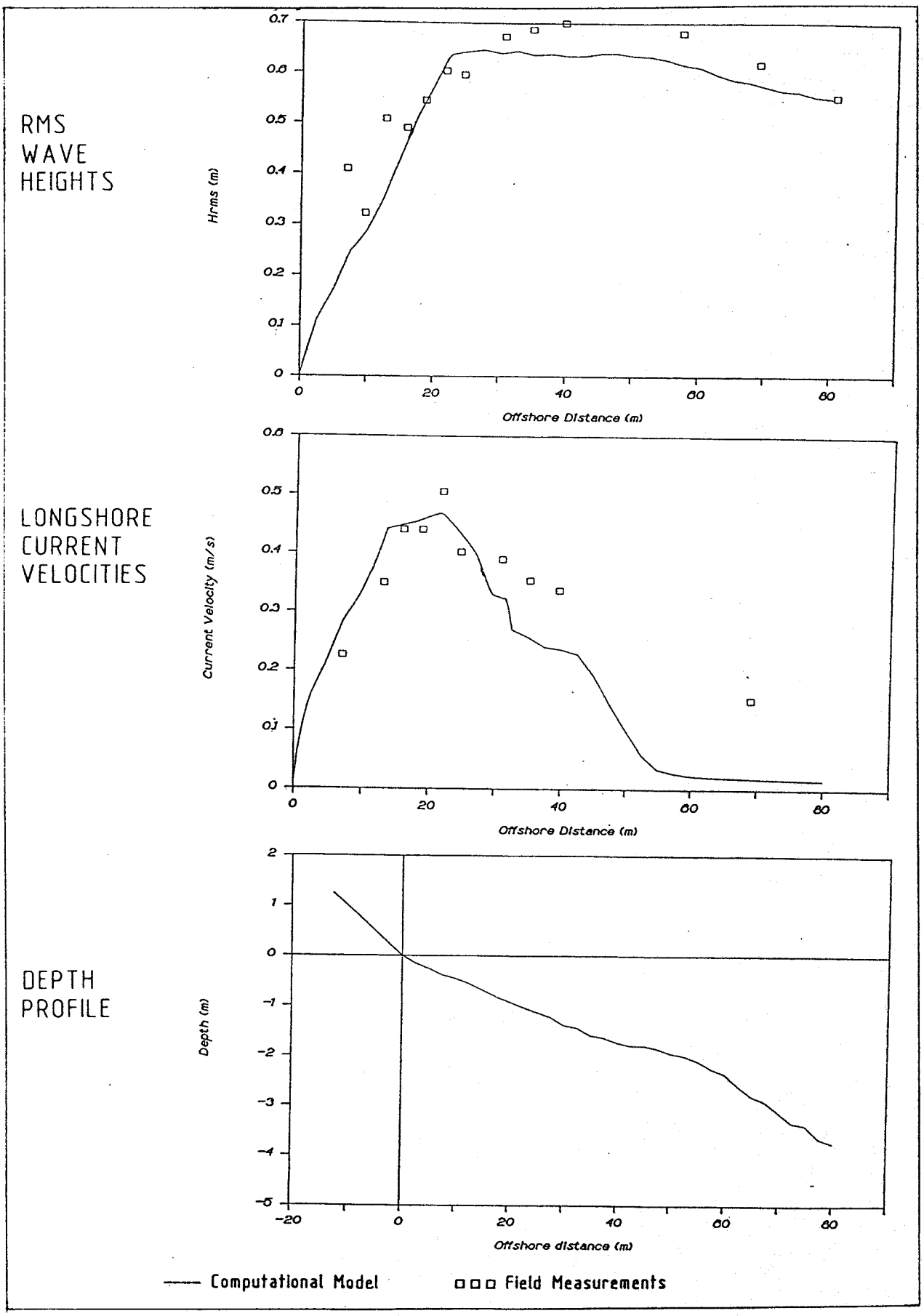

Fig 3 Comparison of Computational Model with Leadbetter Beach Data. Feb 3 1980

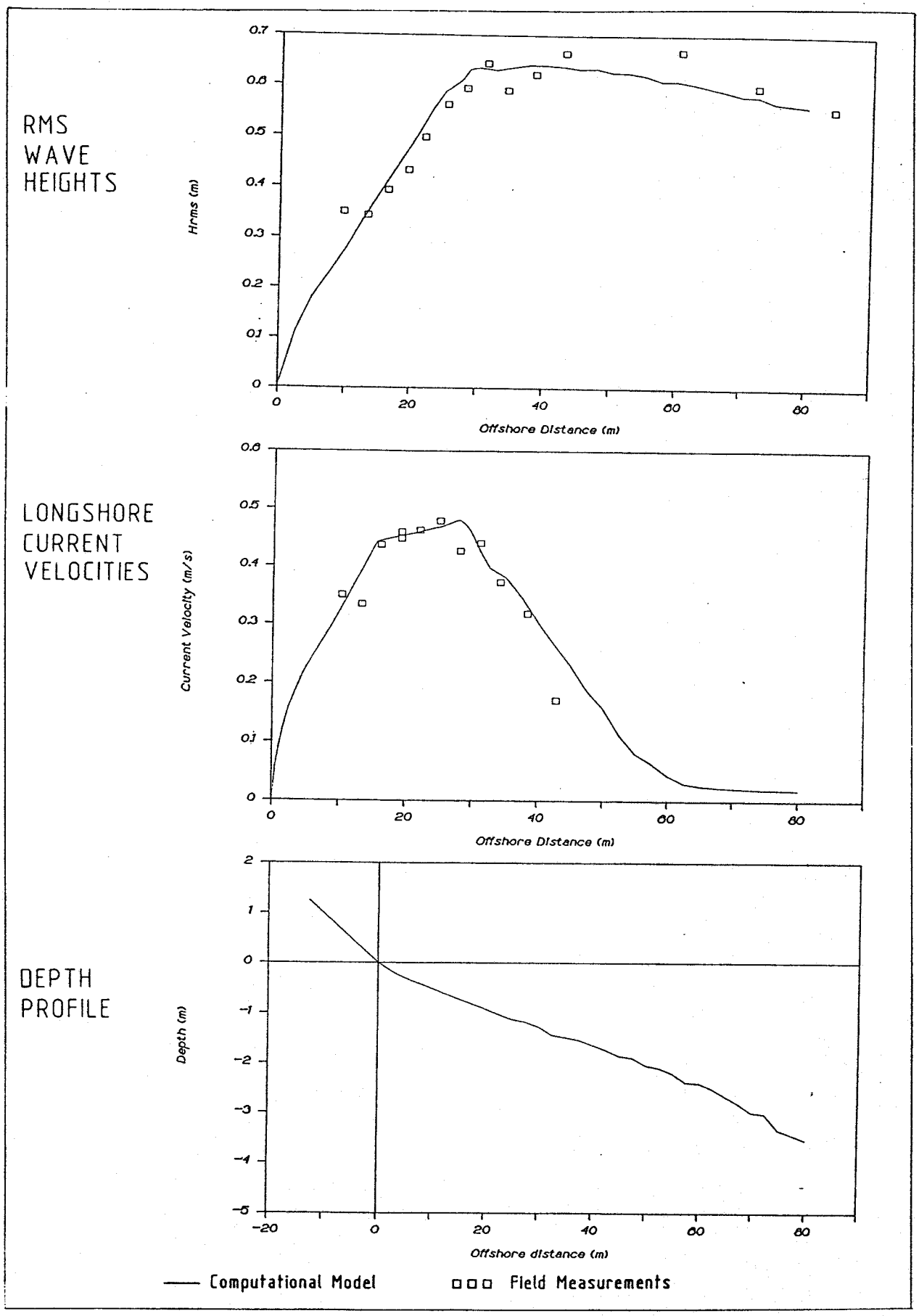

Fig 4 Comparison of Computational Model with Leadbetter Beach Data. Feb 4 1980

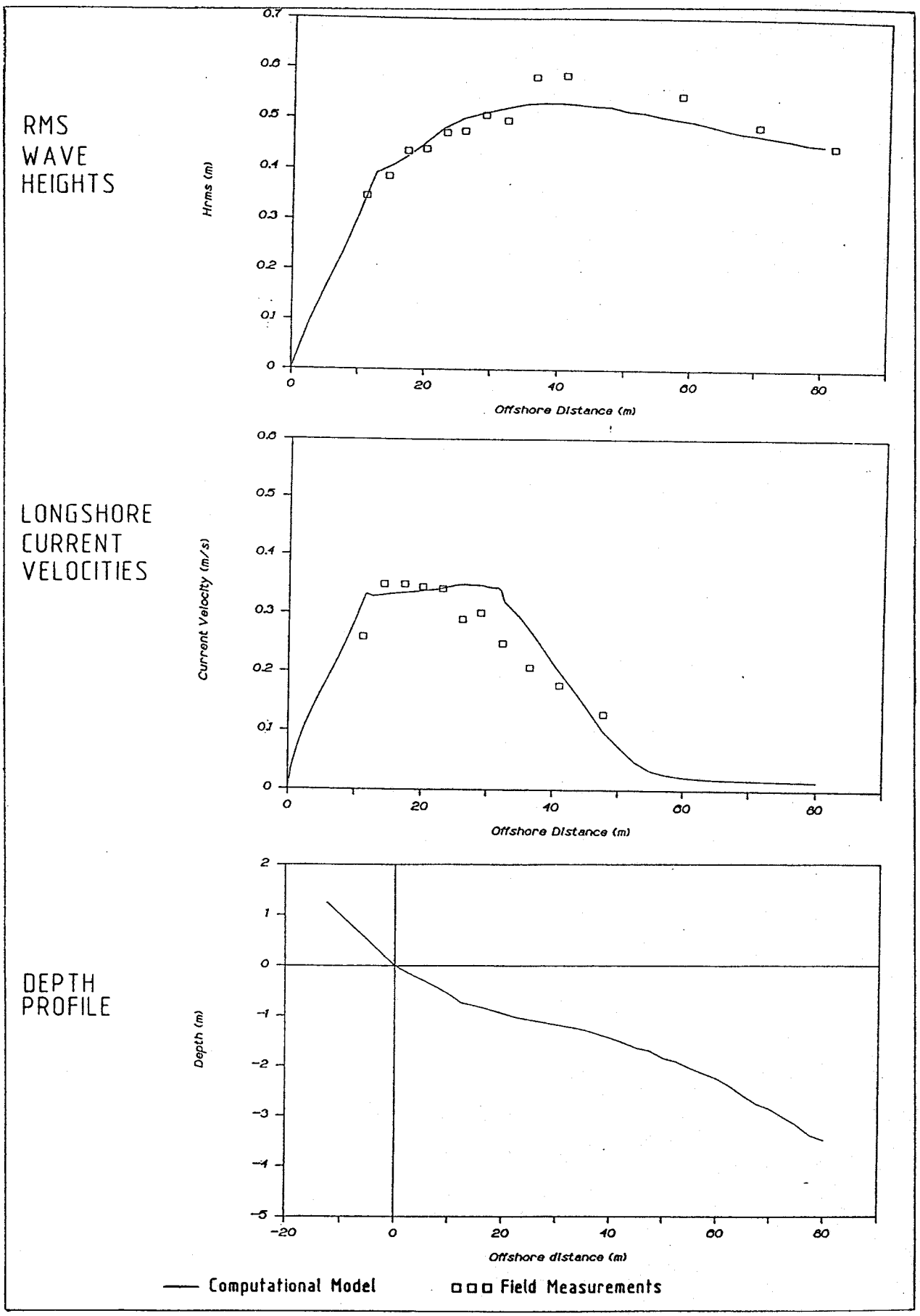

Fig 5 Comparison of Computational Model with Leadbetter Beach Data. Feb 5 1980

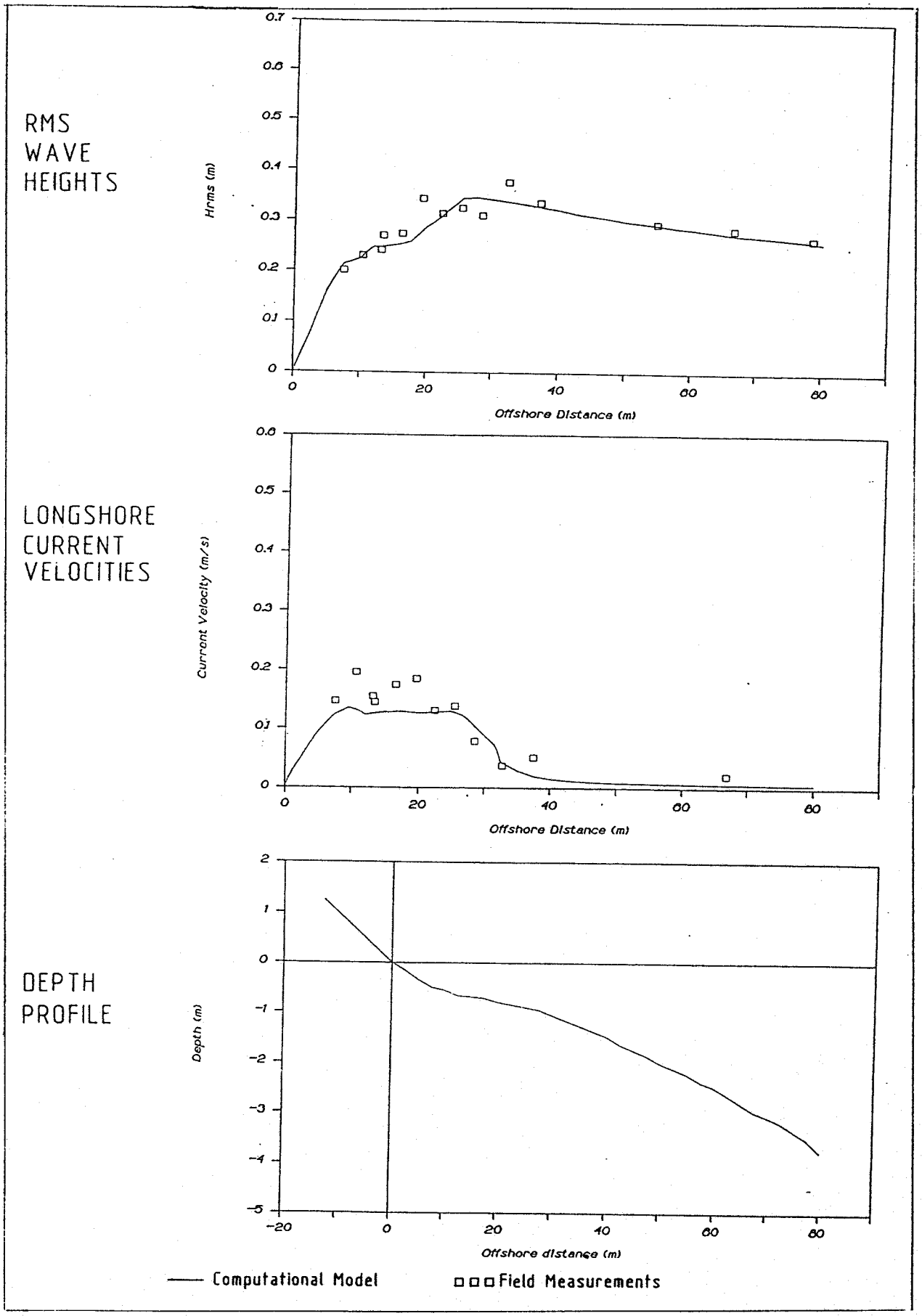

Fig 6 Comparison of Computational Model with Leadbetter Beach Data. Feb 6 1980

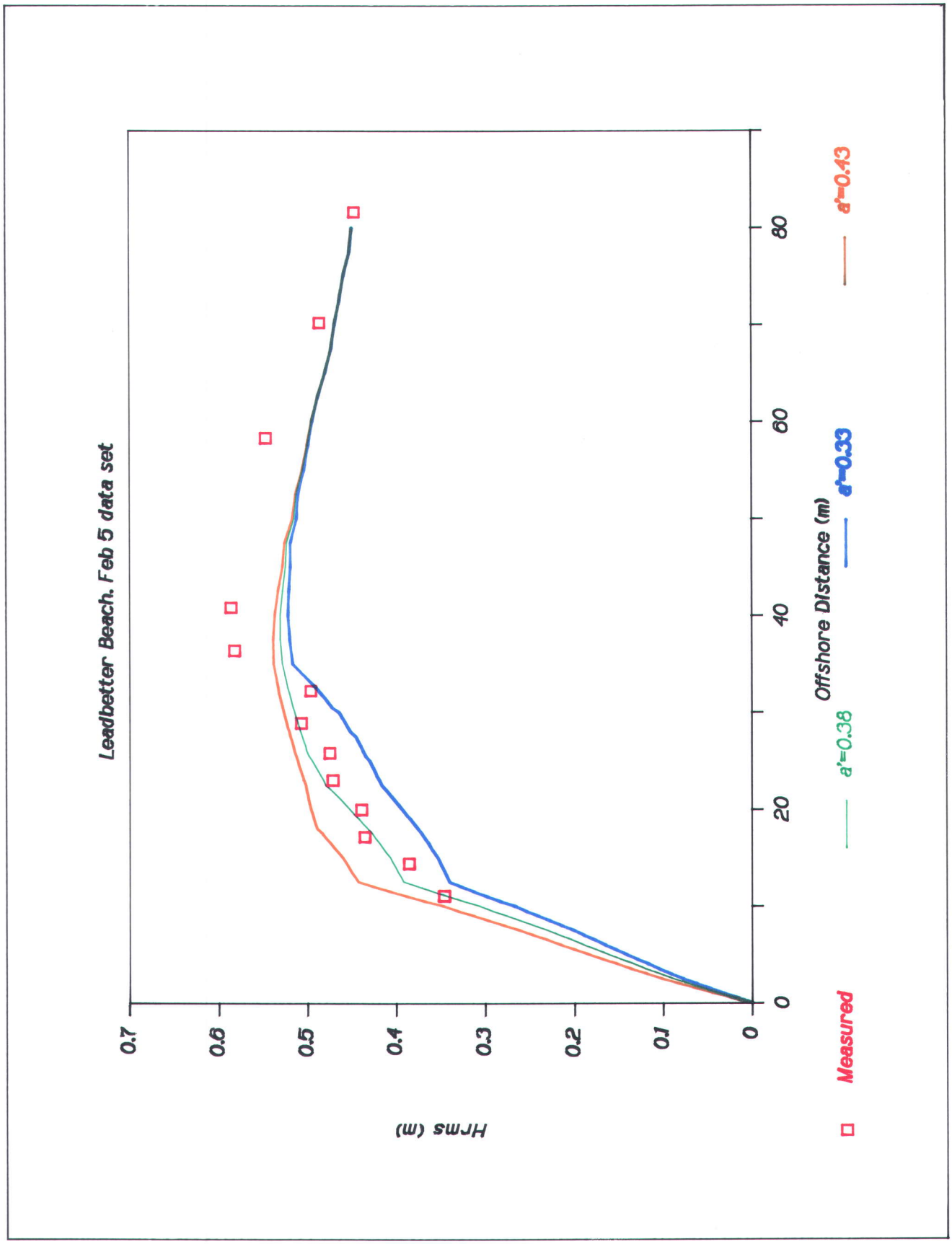

Fig 7 RMS Wave Heights. Effect of varying a' in the Weggel breaker criterion.

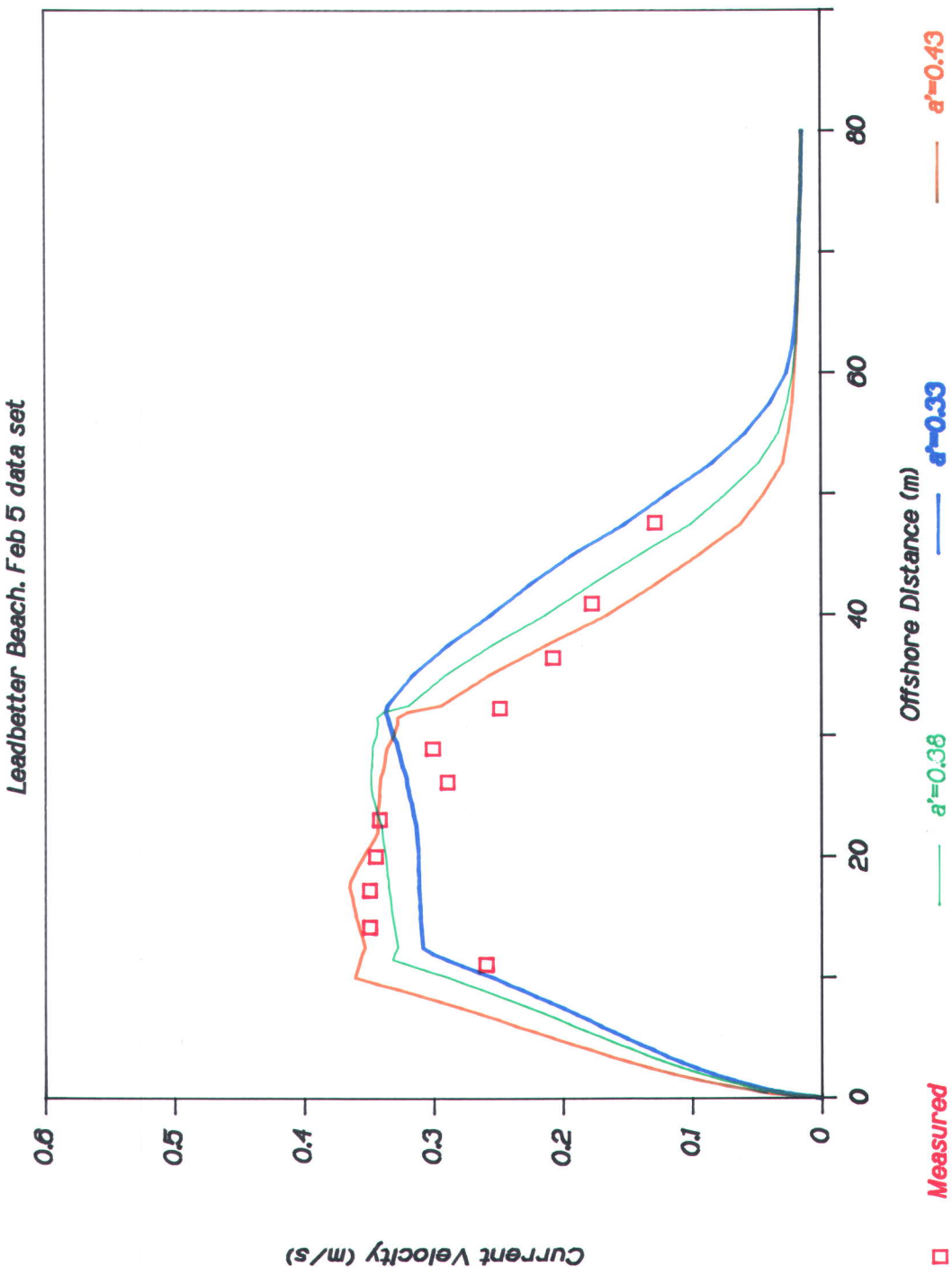

Fig 8 Longshore Current Velocities. Effect of varying a' in the Weggel breaker criterion.

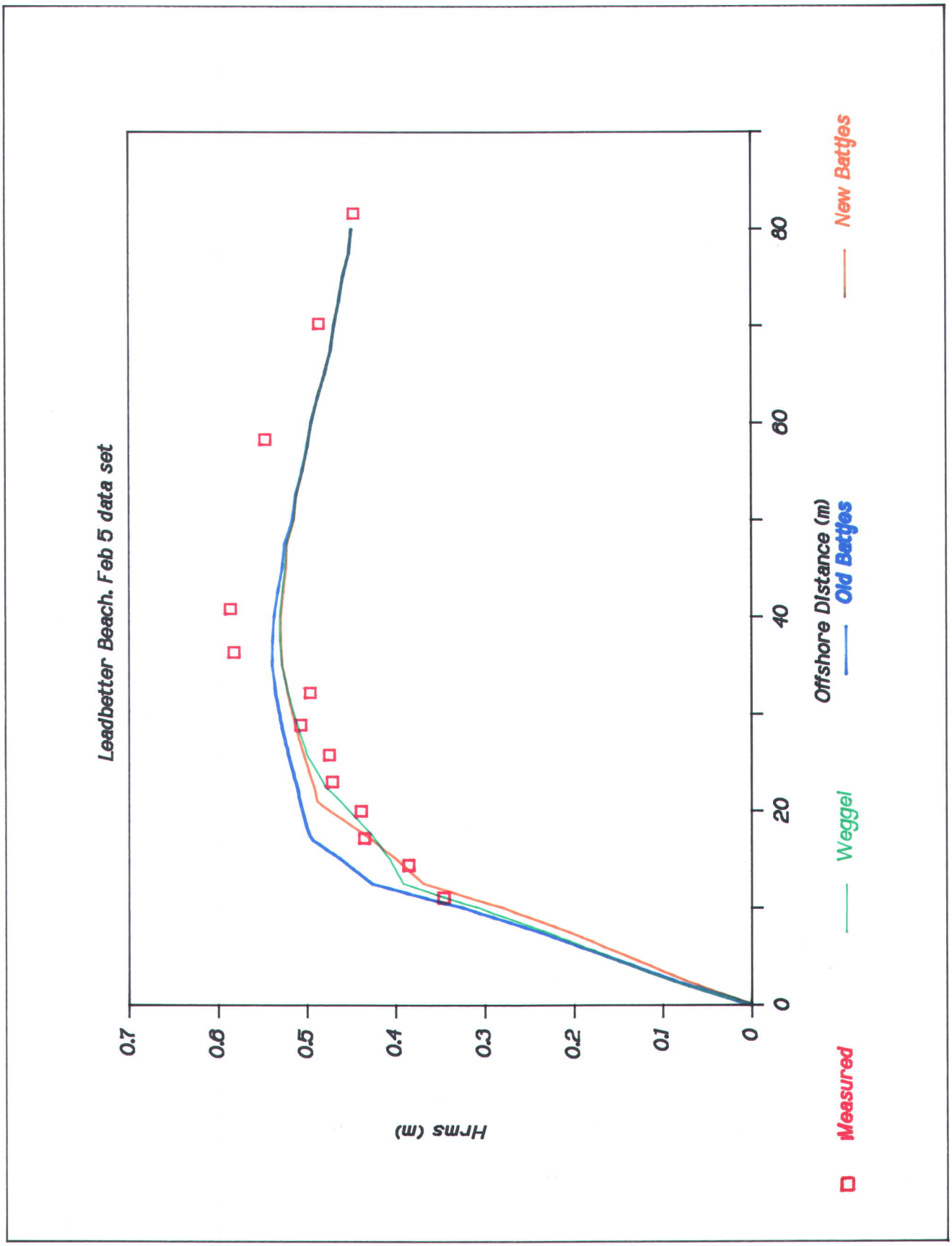

Fig 9 RMS Wave Heights. Weggel, old Battjes and new Battjes breaker criteria.

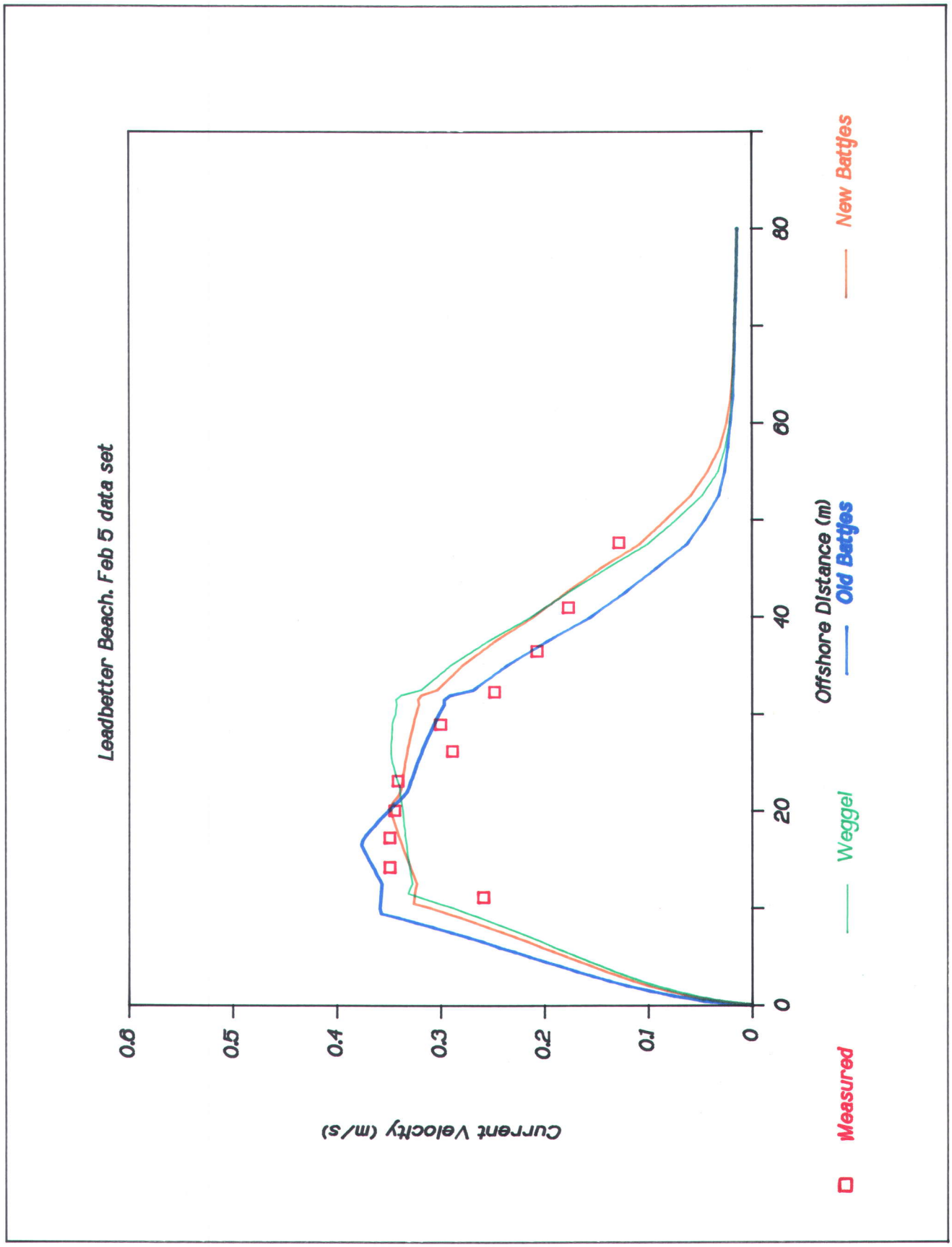

Fig 10 Longshore Current Velocities. Weggel, old Battjes and new Battjes breaker criteria.

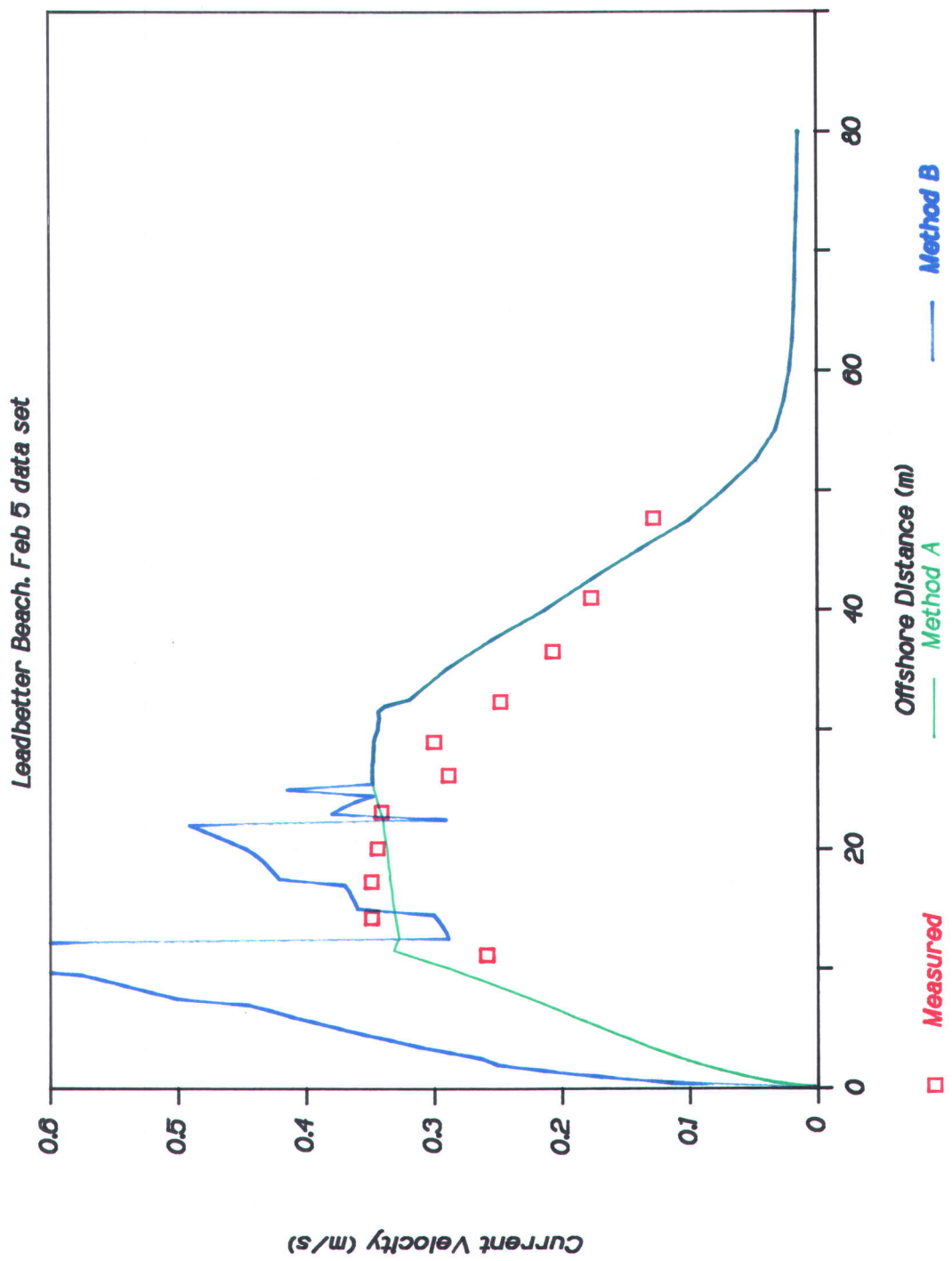

Fig 11 Longshore Current Velocities. Wave energy dissipation rate using Methods A and B.

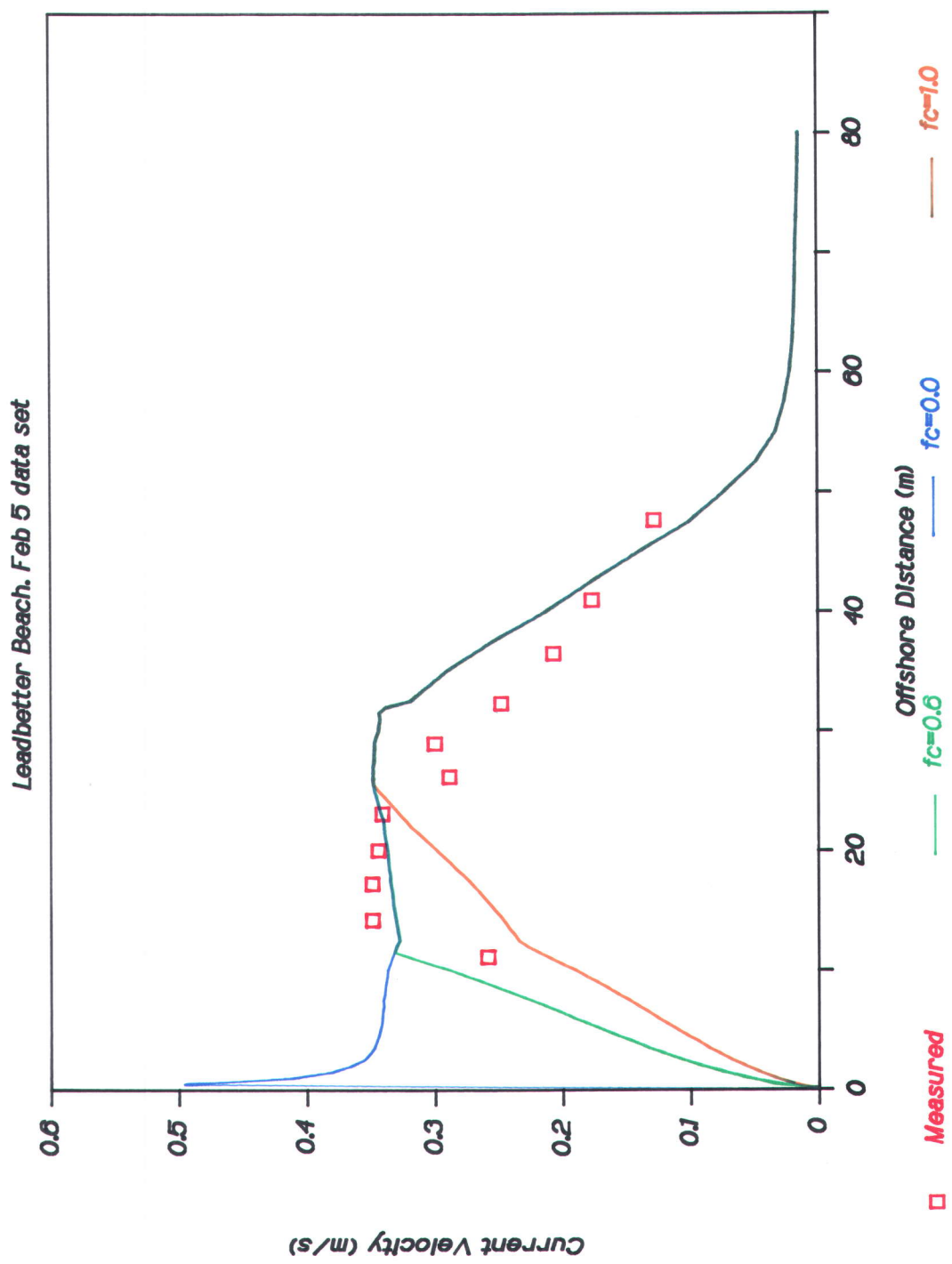

Fig 12 Longshore Current Velocities. Effect of varying fc.

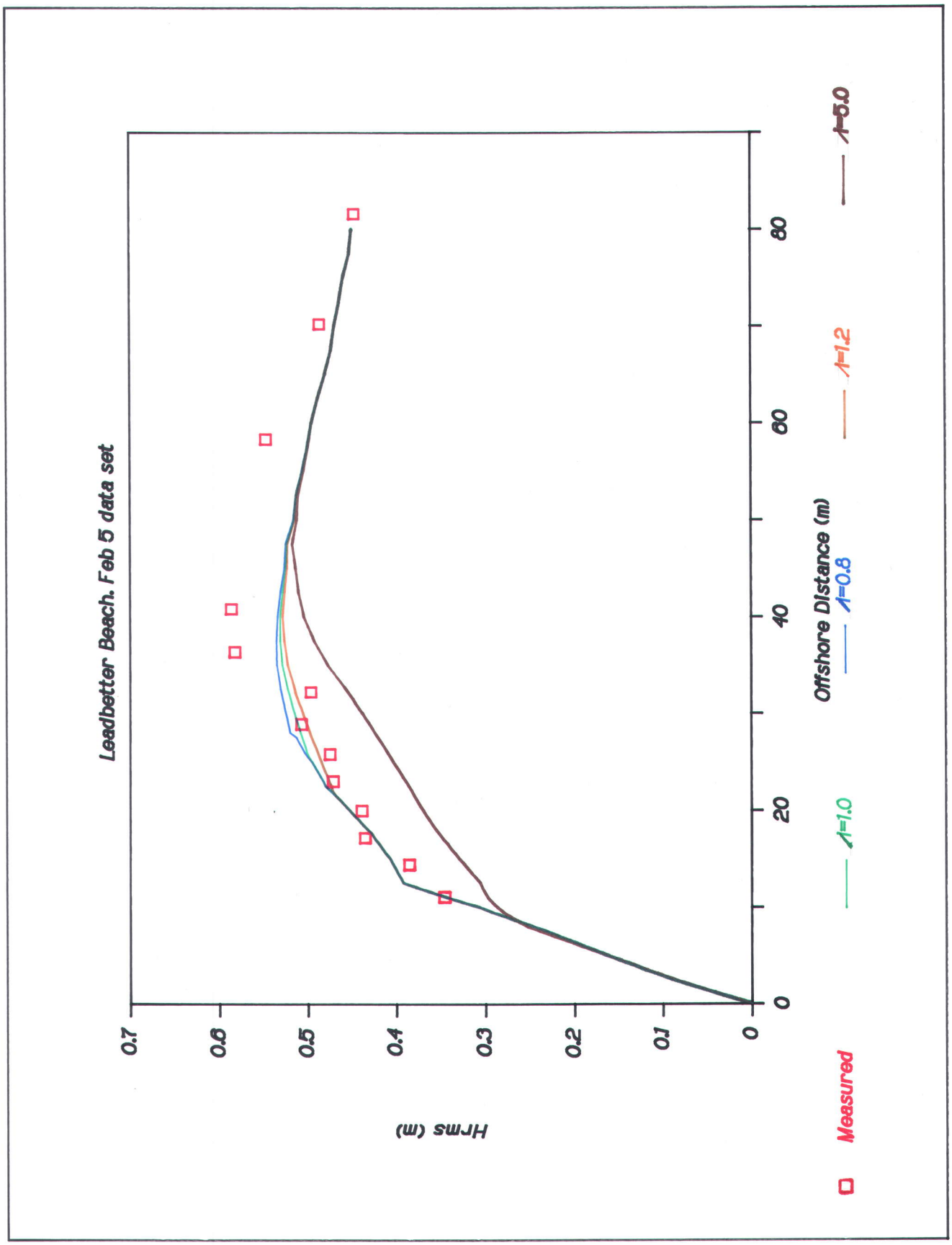

Fig 13 RMS Wave Heights. Effect of varying λ in tidal bore expression.

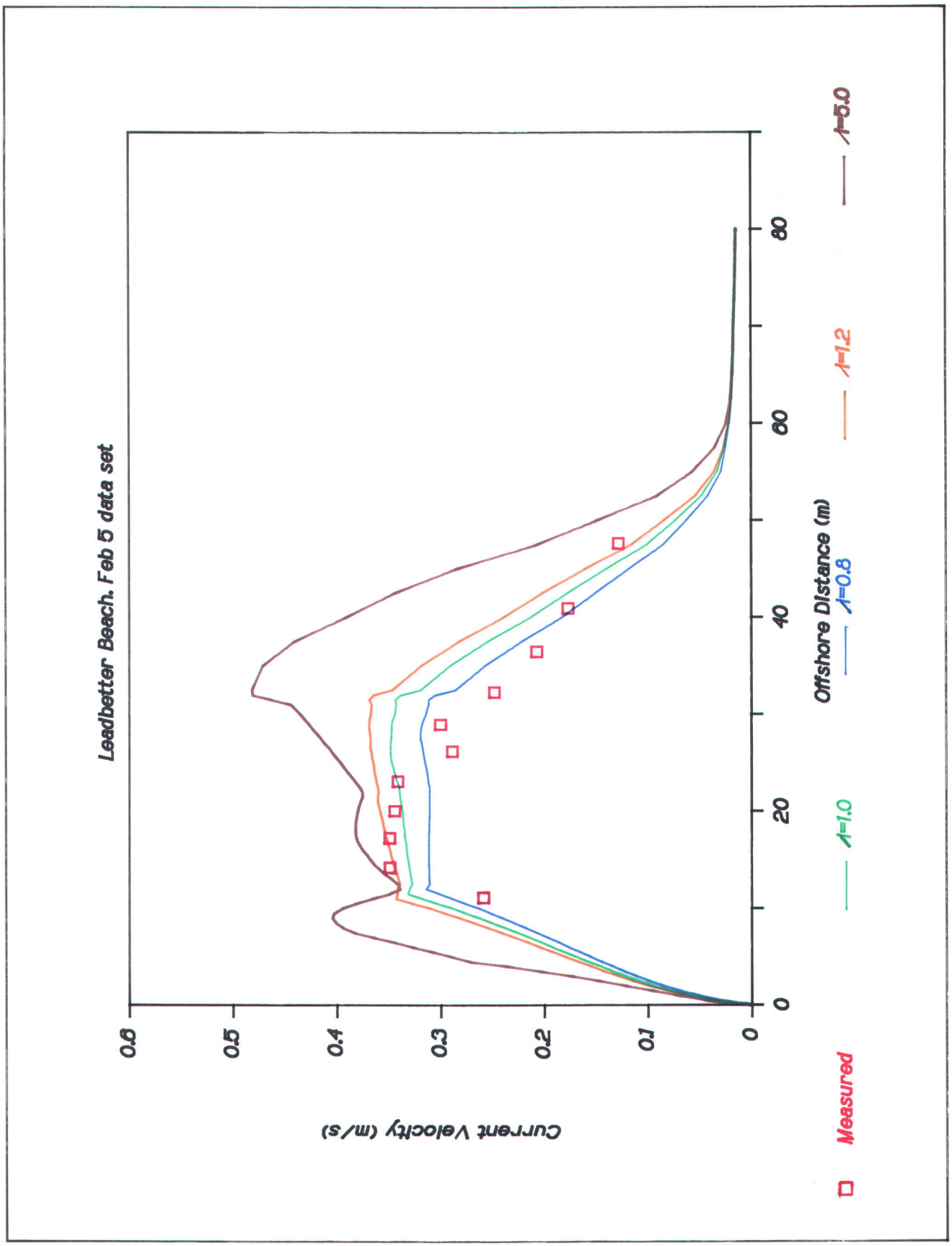

Fig 14 Longshore Current Velocities. Effect of varying λ in tidal bore expression.

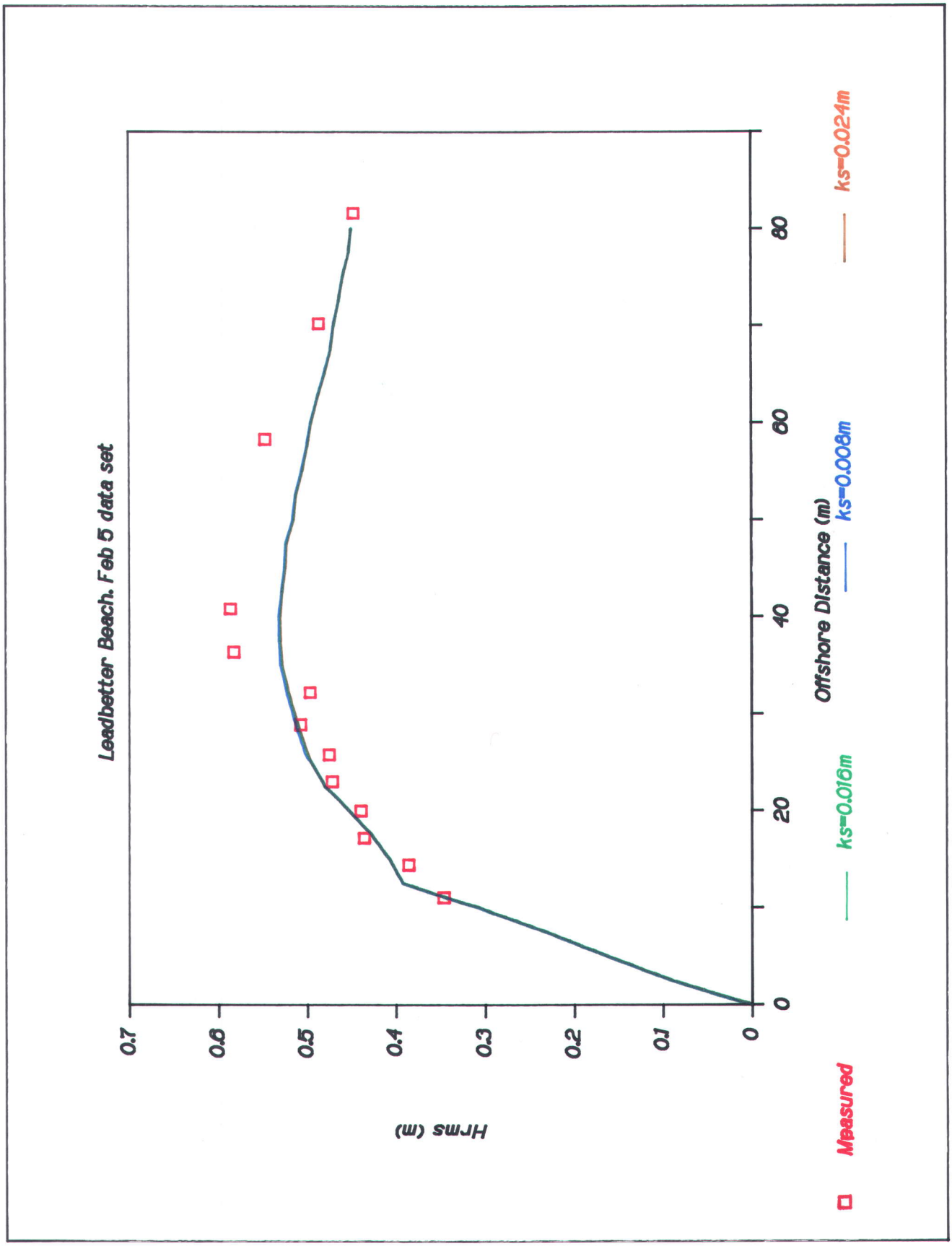

Fig 15 RMS Wave Heights. Different constant ks.

APPENDIX.

A Nearshore Profile Model of Wave and Tidal Current Interaction

Howard N Southgate

Hydraulics Research Ltd, Wallingford, Oxfordshire, UK

Abstract

The theoretical framework of a 1-D model of wave and current interaction in nearshore regions is described in this paper, along with comparisons with laboratory and field data. The theory of wave and current action is based on general mass, energy and momentum equations, applicable inside and outside the surf zone. An important feature is the modelling of tidal currents as well as wave-induced currents, with full interaction between the two types of current and the waves. The model is very efficient computationally and can process large quantities of input wave and tidal data (typically tens or hundreds of thousands of values), making it suitable for the investigation of long-term processes on beaches or in nearshore regions. The model is designed to be used in conjunction with an appropriate sediment transport routine for problems concerned with the longshore movement of sediment.

1. INTRODUCTION

In this paper the theory, computational techniques and validation of a computational model for predicting wave and current conditions in nearshore regions is described. The model uses the approximation of a straight coastline with parallel depth contours, and determines wave and current conditions at grid points along a profile line perpendicular to the

coastline. Currents are assumed to be depth-averaged and parallel to the coastline. The waves are treated as steady, linear and monochromatic in this paper, but the model is capable of being extended to linear random wave spectra.

The model does not attempt a complete representation of surf zone physics, but is intended as a practical tool for solving specific types of engineering problems related to beach and nearshore processes. These problems are those associated with long-term wave and longshore current predictions and longshore sediment movement. For these purposes it is necessary for the model to be capable of analysing many thousands of input wave and tidal data values (for example, a ten-year sequence of hourly wave data involves about 88,000 values).

A balance therefore has to be struck between the inclusion and accurate representation of physical processes on the one hand, and computational speed and efficiency, and flexibility of use on the other. The model achieves computational speed by considering one horizontal dimension only and employing a rapid theoretical method and computing algorithm, particularly in the modelling of longshore currents (Section 3) and the treatment of lateral diffusion of momentum resulting from wave breaking turbulence (Sections 3 and 4). These simplifications allow the inclusion of a fully interactive treatment of waves, longshore wave-induced currents and longshore tidal currents (described in detail in Section 3) while maintaining sufficient computational speed for the analysis of many thousands of input wave and tidal data values.

The model is designed for use on reasonably long and straight stretches of coastline for which the parallel-depth contour assumption is a good approximation. The correctness of this approximation will depend on such factors as the incident wave angle and the offshore distance for which the model is to be used. In general, the approximation will be better for short offshore distances and near-normally incident waves. In practice, the offshore distance can be considerably shortened by using a 2-D refraction model to transform waves to a suitable inshore depth contour, but still located outside the surf zone at all stages of the tide.

The main features of the model are summarised below:

1) Longshore tidal currents, as well as wave-induced currents, are included, with full interaction between the waves and the two types of current. The model is not designed for 2-D flow patterns or cross-shore flows such as undertow or rip currents.

2) The theory is based on general mass, energy and momentum balance equations which are applicable both inside and outside the surf zone. The determination of longshore currents uses an analytical solution to the longshore momentum balance equation.

3) Any depth profile can in principle be used; there is no restriction to monotonically varying depths.

4) Input to the model requires no special field exercise or additional major numerical model study. Suitable input tidal conditions can be obtained from standard Tide Tables, while wave conditions can be

determined by hindcasting from wind data. If measured wave or tidal data are available, they can provide a site-specific calibration or, if sufficiently extensive, an alternative source of input.

5) Tens or hundreds of thousands of input wave and tidal data values can be analysed at reasonable computing cost. This is an important requirement for the long-term predictions of hydrodynamic and morphological processes. The model is also an economical easy-to-use tool for smaller investigations.

6) The model can be used with an appropriate sediment transport formula for problems concerned with the littoral movement of beach and seabed material. This paper, however, concentrates on the hydrodynamic aspects.

The paper is structured as follows: Section 2 describes the background to the model, placing it in the context of alternative models. In Section 3 details are given of the wave and current theory on which the model is based. Sections 4 and 5 contain comparisons of model predictions with laboratory and field data. The main findings and conclusions are summarised in Section 6.

2 BACKGROUND

A range of computational modelling techniques is presently available for the prediction of inshore hydrodynamic conditions and morphological processes. Wave refraction models based on ray tracing over the coastal area of interest have been used for many years in nearshore wave prediction

problems. Early models of this type are described in Skovgaard et al (1975) and Abernethy and Gilbert (1975). More recent models, including the effects of currents on wave refraction are reported in Jonsson and Christofferson (1984) and Treloar (1986). Townend and Savell (1984) discuss the use of ray tracing models in present engineering practice.

These refraction models have often been combined with one-line beach plan shape models for the prediction of erosion and accretion rates caused by the longshore drift of beach material. Examples of this type of model are described in Price et al (1972), Komar and Inman (1970) and Ozasa and Brampton (1980). A recent assessment of the engineering uses of these models is given in Brampton and Motyka (1987). The representation of physical processes in these models is very simplified with no tidal effects or wave-current interactive effects. Furthermore, wave-induced current and sediment transport quantities are calculated only as single average values across the inter-tidal and surf zones. However, because of their simplicity, one-line models are suitable for analysing large sequences of wave data and therefore for investigating long-term beach processes.

A considerable amount of research effort has been devoted to extending refraction models to incorporate other wave processes such as refraction by currents, diffraction, wave reflections, bottom friction, wave breaking and wind growth. Examples of these models are to be found in Booij (1981), Kirby (1984), Dalrymple et al (1984) and Booij et al (1985). Models have also been developed to analyse the transformation of wave spectra rather than waves with a single period and direction. Abernethy and Gilbert (1975), Booij et al (1985) and Treloar (1986) describe different approaches to the modelling of spectral transformation. Recently, sophisticated 2-D

and 3-D models of the nearshore zone have been developed to analyse the interaction of waves, currents and sediment transport (eg Hubertz (1984), Wind and Vreugdenhil (1986), Stive and de Vriend (1987) and Yoo and O'Connor (1986)). Such types of model give detailed results of the hydrodynamic and morphological conditions, but have a high computing requirement which limits the number of input conditions that can be tested.

The model described in this paper attempts to fill an engineering need not covered by refraction/one-line models or the 2-D and 3-D nearshore models. This need is for long-term predictions of waves, longshore currents and longshore sediment transport rates. The model improves on one-line beach plan shape models by the incorporation of a fully interactive modelling of waves and currents including tidal currents, while having a much greater computational speed than the 2-D and 3-D nearshore models enabling many thousands of input data values to be analysed.

3 THEORY OF WAVE AND CURRENT MODELLING

3.1 Introduction

The model is fully interactive, with waves influencing the current field through seabed friction and the generation of longshore currents, and currents influencing the wave field through seabed friction and refraction. Alternate calls are made from a master program to separate wave and current modules, with updated values of the wave and current parameters being passed between the modules. These calls are made up to a maximum number at which the values of the wave and current parameters have converged.

3.2 Wave Modelling

The incorporated wave processes are shoaling, refraction (by depth variations and currents), seabed friction and wave breaking. Wave radiation stresses are calculated, which form the basis for a determination of wave-induced longshore currents and set-up of the still water level. Input wave conditions are supplied at the grid point furthest offshore in the form of a representative height, period and direction. A tide level is input and is assumed to be the same for all grid points.

In the calculation of kinematic quantities, the principal equation to be solved at each grid point is the dispersion relation in the presence of currents,

$$\omega_a - Uk \cos(\delta-\alpha) = (gk \tanh kh)^{1/2} \qquad (1)$$

The wavenumber, k, is determined from Eq 1 in terms of known values of the absolute wave angular frequency ω_a, the longshore current velocity U, the current direction δ, the wave orthogonal direction α, the acceleration due to gravity g, and the water depth h. Angle quantities are defined in Fig 1. Once k is known, the following related quantities can be calculated,

a) Relative wave angular frequency

$$\omega_r = \omega_a - Uk \cos\alpha \qquad (2)$$

b) Relative wave celerity

$$c_r = \frac{\omega_r}{k} \tag{3}$$

c) Relative group velocity

$$c_{gr} = \frac{\omega_r}{2k}\left(1 + \frac{2kh}{\sinh(2kh)}\right) \tag{4}$$

d) Absolute group velocity (the vector sum of U and c_{gr}. See Fig 1)

$$c_{ga} = (U^2 + c_{gr}^2 + 2Uc_{gr}\ \mathrm{Cos}\ (\delta-\alpha))^{1/2} \tag{5}$$

e) Ray direction (see Fig 1)

$$\mu = \tan^{-1}\left(\frac{U\ \mathrm{Sin}\ \delta + c_{gr}\ \mathrm{Sin}\ \alpha}{U\ \mathrm{Cos}\ \delta + c_{gr}\ \mathrm{Cos}\ \alpha}\right) \tag{6}$$

In order to derive kinematic quantities at the grid point under study (subscript i), given quantities at the previous point (subscript o), Snell's law for the orthogonal direction is used:

$$\mathrm{Sin}\ \alpha_i = \frac{k_o}{k_i}\ \mathrm{Sin}\ \alpha_o \tag{7}$$

This equation is then used with Eqs 1-6 to predict the kinematic quantities at the point under study.

Determination of wave dynamics is based on integration of the wave action equation (Christoffersen and Jonsson, 1980),

$$\frac{d}{dy}\left(\frac{E\, c_{ga}\, \mathrm{Cos}\, \mu}{\omega_r}\right) = -\frac{(D_f + D_b)}{\omega_r} \tag{8}$$

in which y is the co-ordinate in the onshore direction (Fig 1), E is the wave energy density, and D_f and D_b are the spatial wave energy flux dissipation rates due to seabed friction and wave breaking respectively. For linear monochromatic waves, E is related to the wave height H by,

$$E = \frac{1}{8}\rho g H^2 \tag{9}$$

in which ρ is the water density. Integration of Eq 8 provides the means of determining the wave height at a grid point in terms of quantities at the preceding point. In order carry out this integration, explicit expressions for D_f and D_b are needed.

The method of determining seabed frictional dissipation is based on the boundary layer model of O'Connor and Yoo (1988) which extends the work by Bijker (1966). One result of this method is that the interacted frictional dissipation is manifested through an enhancement of the separate wave and current friction factors, thereby allowing wave and current energy dissipation rates to be treated independently. O'Connor and Yoo (1988) have shown that D_f is given to a good approximation by $D_f = \langle \tau_w V \rangle$ where τ_w is the instantaneous wave bed shear stress (i.e. the oscillating part), V is the instantaneous wave bottom orbital velocity, and $\langle\ \rangle$ denotes averaging

over a wave period (see also Christoffersen and Jonsson (1985)). O'Connor and Yoo then show that this expression for D_f leads to the form,

$$D_f = \rho \, C_{fw} \, V_o^3 \tag{10}$$

where C_{fw} is a wave friction factor including an enhancement resulting from the interaction with the current field. V_o is the maximum wave orbital velocity at the seabed, which for linear monochromatic waves is related to the wave height, H, by

$$V_o = \frac{H \, \omega_r}{2 \sinh (kh)} \tag{11}$$

The method of determining the breaking energy dissipation rate is based on Battjes and Janssen (1978). The first step in this method is the determination of the wave height at which breaking starts to occur, for given water depth, bed slope and wave characteristics. In the present work a modification of an empirical formula put forward by Weggel (1972) and recommended by the CERC Shore Protection Manual is used.

$$H_b = \frac{ah}{1 + bh/(gT^2)} \tag{12}$$

in which

$$a = \frac{2a'}{1 + \exp(-19.5m)} \tag{13}$$

$$b = 43.75 \, (1 - \exp(-19m)) \tag{14}$$

In Eqs 12-14, H_b is the breaker wave height, T the absolute wave period, m the beach slope, and a' an empirically determined parameter. In Weggel's original formula a' was set to 0.78, but it was found necessary in this work to increase the value of a', which has the effect of delaying the onset of breaking. The reasons for the choice of a' are discussed in Section 4.

Once the breaker height has been calculated at a particular location, the probability of occurrence of broken waves needs to be determined. For monochromatic waves this probability is one for $H \geq H_b$ and zero for $H \leq H_b$. For applications where the longshore currents, rather than the wave heights, are of principal interest, it is necessary to have a means of modelling the lateral diffusion of momentum under breaking waves which gives rise to a smooth cross-shore distribution of longshore current velocities. In this model lateral diffusion is not treated explicitly but is simulated by the similar smoothing that results from considering random wave input. Previous investigations (Battjes, 1972 and Thornton and Guza, 1986) have concluded that computational models which employ this method provide sufficiently accurate predictions of longshore current velocities under random waves for practical purposes. For monochromatic wave input, the model uses a simulation of random wave breaking for the purpose of determining the cross-shore distribution of radiation stress driving forces, but treats the waves as monochromatic in all other respects. In the comparison with experimental data in Section 4, it is shown that this method gives comparable accuracy in its predictions of longshore current velocities to alternative models which include an explicit representation of lateral diffusion (Yoo and O'Connor, 1987, Pechon, 1987, Bonneton and Gaillard, 1985). The present method provides savings in computing effort and avoids the need of determining an eddy viscosity coefficient.

The Rayleigh distribution of wave heights is used in the simulation of breaking of random waves,

$$P(H)\ dH = \frac{2H}{H_{rms}^2} \exp(-H^2/H_{rms}^2)\, dH \qquad (15)$$

In this equation H is a general wave height, H_{rms} the root-mean-square wave height, and P(H)dH the probability of occurrence of a wave height lying in the range dH centred on H. In shallow water, the Rayleigh distribution is truncated at the breaker height, H_b, and therefore some assumption has to be made about the probability distribution of the broken wave energy. Battjes and Janssen make the simple but physically plausible assumption that all broken waves have a wave height equal to H_b, resulting in a probability distribution truncated at H_b to represent unbroken waves, but with an additional delta function at H_b representing the broken waves. With this assumption it can be shown that the probability of occurrence of broken waves, Q, is related to H_{rms} and H_b by (Battjes and Janssen, 1978),

$$\frac{1 - Q}{(-\ln Q)} = \left(\frac{H_{rms}}{H_b}\right)^2 \qquad (16)$$

For the rate of dissipation of broken wave energy, D_b, an expression is used for energy dissipation in a tidal bore from which can be derived for D_b,

$$D_b = \frac{\lambda\, \rho\, g^{3/2}\, k\, H_b^3\, Q}{8\pi\, h^{1/2}} \qquad (17)$$

in which λ is an empirical constant of the order one, expressing the difference between the tidal bore and wave breaking processes. Using Eq 16, D_b can be expressed in terms of H_{rms},

$$D_b = \frac{\lambda \rho g^{3/2} k H_{rms}^3 f(Q)}{8\pi h^{1/2}} \tag{18}$$

$$\text{where } f(Q) = Q\left(\frac{-\ln Q}{1-Q}\right)^{3/2} \tag{19}$$

Expressions for D_f (Eq 10) and D_b (Eq 18) have been obtained and it is now possible to integrate the wave action equation (Eq 8). Making the substitutions and rearranging the equation,

$$\frac{1}{H^3}\frac{d}{dy}\left(\frac{H^2 c_{ga} \text{Cos}\mu}{\omega_r}\right) = -\left[\frac{C_{fw} \omega_r^2}{g \text{Sinh}^3(kh)} + \frac{\lambda g^{1/2} k f(Q)}{\pi \omega_r h^{1/2}}\right] \tag{20}$$

in which in the expression for broken waves H has been interpreted as H_{rms}. Eq 20 can be integrated between one grid point (subscript o) and the following one (subscript i) using the method in Southgate (1987) to give,

$$H_i = H_o K_s K_r K_d \left(\frac{1}{1 + \beta H_o}\right) \tag{21}$$

$$\text{where } K_s = \left(\frac{c_{gao}}{c_{gai}}\right)^{1/2} \qquad \text{Shoaling Coefficient} \tag{22}$$

$$K_r = \left(\frac{\cos \mu_o}{\cos \mu_i}\right)^{1/2} \qquad \text{Refraction Coefficient} \qquad (23)$$

$$K_d = \left(\frac{\omega_{ri}}{\omega_{ro}}\right)^{1/2} \qquad \text{Doppler Coefficient} \qquad (24)$$

$$\beta = \tfrac{1}{2}\left(\frac{c_{gao}\cos\mu_o}{\omega_{ro}}\right)^{1/2} \int_{y_o}^{y_i} \left(\frac{\omega_r}{c_{ga}\cos\mu}\right)^{3/2} \left[\frac{C_{fw}\,\omega_r^2}{g\,\sinh^3(kh)} + \frac{\lambda\, g^{1/2} k\, f(Q)}{\pi\, \omega_r\, h^{1/2}}\right] dy \qquad (25)$$

The merit of this method of integration is that most of the H-dependence has been removed from the integral in Eq 25. This integral is evaluated at successive grid points by the trapezium rule. Both C_{fw} and f(Q) are still dependent on H, but relatively weakly, and a more accurate evaluation of H can be made by iteration. Typically, three runs (two iterations) have been found to give convergence of H at all grid points to around 1% at worst.

Onshore and longshore components of the wave radiation stress are determined in the model. The onshore component, S_{yy}, is given by the formula for progressive waves,

$$S_{yy} = \frac{1}{8}\rho g\, H^2 \left[\left(\frac{2\, c_{gr}}{c_r} - \tfrac{1}{2}\right) \cos^2\alpha + \left(\frac{c_{gr}}{c_r} - \tfrac{1}{2}\right) \sin^2\alpha\right] \qquad (26)$$

The wave-induced set-up, η, is calculated from the equation for the time-mean momentum balance in the onshore direction, neglecting the small contribution from the mean bottom shear stress (Stive and Wind, 1982),

$$\frac{d\eta}{dy} = - \frac{1}{\rho g \ (h+\eta)} \frac{dS_{yy}}{dy} \tag{27}$$

η is determined at any grid point (subscript i) in terms of its value at the preceding grid point (subscript o) using a finite difference formulation of Eq 27.

$$\frac{\eta_i - \eta_o}{\Delta y} = - \frac{1}{\rho g \ (h + (\eta_i + \eta_o)/2)} \frac{\Delta S_{yy}}{\Delta y} \tag{28}$$

Eq 28 is a quadratic in η_i with solution,

$$\eta_i = -h + \left[(h+\eta_o)^2 - \frac{2\Delta S_{yy}}{\rho g}\right]^{1/2} \tag{29}$$

in which $\Delta S_{yy} = S_{yyi} - S_{yyo}$, $\Delta y = y_i - y_o$ and $h = (h_i + h_o)/2$. This method of solution is valid in very shallow water where the wave set-up is a non-negligible proportion of the total depth.

The wave radiation stress in the longshore direction, S_{xy}, is given to second order in H by (Longuet-Higgins, 1970),

$$S_{xy} = \frac{\rho g \ H^2 \ c_{gr} \ \mathrm{Sin}2\alpha}{16 \ c_r} \tag{30}$$

It was noted by Longuet-Higgins that the irrotational part of S_{xy} remains unchanged by depth refraction and shoaling, and the only changes to S_{xy} arise from dissipative processes. For diffraction, and refraction by currents, S_{xy} does in general change, but not for the special case of a straight coastline with parallel depth contours considered in this model. Therefore the only changes to S_{xy} are those due to the dissipative processes of bottom friction and, principally, wave breaking. It was shown in Southgate (1987) that,

$$S_{xyi} = \epsilon^2 \, S_{xyo} \tag{31}$$

where ϵ is the ratio of the wave height at the inshore point calculated with dissipative processes to that calculated without dissipative processes. From Eq 21, ϵ is given by,

$$\epsilon = \frac{1}{1 + \beta H_o} \tag{32}$$

The radiation stress gradient provides the driving force for the wave-induced current in the longshore direction and is given, per unit sea area, by

$$F = - \frac{dS_{xy}}{dy} \tag{33}$$

3.3 Current Modelling

Tidal and wave-induced currents in the longshore direction are determined by solving the longshore momentum balance equation. The tidal currents are generated by longshore variations in the water-surface level (ie pressure-generated), and balanced by seabed friction and inertia. The wave-induced currents are generated by spatial gradients of the wave radiation stresses, again balanced by seabed friction and inertia. Interaction between the two types of currents, and between them and the waves, is incorporated. The method provides coupled analytical expressions for the steady and tidal-oscillatory current velocities. The influence of inertia in the tidal currents, relative to that of seabed friction, varies significantly across the modelled region, so a quasi-steady treatment of tidal currents is not adequate. The effects of inertia are modelled explicitly in the present method.

All currents are assumed to be depth-averaged and in the longshore direction (x-direction). Therefore no onshore-offshore currents such as rip currents or undertow are modelled. Some quantities such as the maximum water surface elevation, ζ_m, are allowed a variation in the x-direction on a large length scale (of the order of a tidal wavelength, typically about 500km), but locally they are regarded as constant in x. Wherever an x dependency is shown, the variation in x is understood to be on the large length scale. This assumption is consistent with the continuity (or mass conservation) equation

$$\frac{\partial}{\partial t}(h+\zeta) + \frac{\partial}{\partial x}[(h+\zeta)U \sin\delta] + \frac{\partial}{\partial y}[(h+\zeta)U \cos\delta] = 0 \qquad (34)$$

at the local length scale.

A general sinusoidal form is assumed for the surface elevation above mean sea level, ζ, with an additional time-independent term, ζ_o, to account for any asymmetry in the tidal pressure driving force,

$$\zeta = \zeta_m(x) \exp(i[\omega t - \phi(x)]) + \zeta_o(x) \tag{35}$$

in which ω is the tidal angular frequency, t is time, ζ_m is the maximum surface elevation of the oscillatory part, and ϕ is a general phase function.

The longshore water surface slope, S, is related to ζ through its definition

$$S = \frac{\partial \zeta}{\partial x} \tag{36}$$

This definition implies that S also has a sinusoidal form plus a time-constant term, S_o,

$$S = S_m(x) \exp(i[\omega t - \Theta(x)]) + S_o(x) \tag{37}$$

in which S_m is the maximum longshore water surface slope and Θ is a general phase function. The relations between S_m, Θ, S_o and ζ_m, ϕ, ζ_o are found by substitution in Eq 36,

$$S_m^2 = \left(\frac{\partial \zeta_m}{\partial x}\right)^2 + \left(\zeta_m \frac{\partial \phi}{\partial x}\right)^2 \tag{38}$$

$$\Theta = \phi + \tan^{-1} \left[\frac{\zeta_m \, \partial\phi/\partial x}{\partial\zeta_m/\partial x}\right] \tag{39}$$

$$S_o = \frac{\partial\zeta_o}{\partial x} \tag{40}$$

ϕ is chosen arbitrarily, the usual convention being to set ϕ to zero at high water. ζ_m, $\partial\zeta_m/\partial x$, $\partial\phi/\partial x$ and S_o are the input quantities required by the model to determine the pressure driving force for the tidal currents, and are assumed to be the same at all cross-shore points (no y-dependence). For reasonably straight stretches of coastline these quantities can be deduced from information contained in Tide Tables.

For the longshore current velocity, U, a general sinusoidal form is assumed, with an additional time-independent current, U_o, to represent the steady component of the tidal current and the (quasi-) steady wave-induced current.

$$U = U_m(x,y) \exp\,(i[\omega t - \varphi(x,y)]) + U_o(x,y) \tag{41}$$

in which U_m is the maximum of the oscillatory component of the longshore current velocity, and φ is a general phase function. U_m can vary in the cross-shore direction. It is assumed that the wave-induced current remains steady (apart from random fluctuations) over the time period during which significant changes to the oscillatory tidal currents take place (one or two hours). Wave-induced currents will show systematic variations over a longer timescale, and for this reason they are termed "quasi-steady".

The seabed shear stress, τ, is determined from the quadratic friction law,

$$\tau = \rho C_{fc} U|U| \tag{42}$$

in which C_{fc} is the current friction factor, including the effects of wave interaction, and is determined by the method of O'Connor and Yoo (1988). In the absence of wave activity, C_{fc} is calculated from the empirical formula of Bijker (1966),

$$C_{fc} = 0.016\ (h/k_s)^{-1/3} \qquad \text{(No wave interaction)} \tag{43}$$

in which k_s is the seabed roughness height.

The longshore current velocity is determined by solving the longshore momentum balance equation. For a combination of oscillatory and steady forces, this is

$$\underset{\text{Inertia}}{\frac{\partial U}{\partial t}} + \underset{\substack{\text{Pressure}\\ \text{Force}}}{gS} + \underset{\substack{\text{Seabed}\\ \text{Friction}}}{\frac{\tau}{\rho h}} = \underset{\substack{\text{Wave Radiation}\\ \text{Stress}}}{\frac{F}{\rho h}} \tag{44}$$

These terms represent the most important forces. In nearshore regions Coriolis forces are generally much smaller, and the non-linear advective terms are locally zero under the 1-D approximation. The treatment of the lateral diffusion of momentum resulting from turbulence under breaking waves is discussed in Section 4. The wave-induced driving force, F, is determined from Eq 33. Quasi-steady driving forces from other sources, such as wind

stress, could also be included on the right-hand side of Eq 44. These are not considered in this paper but represent a possible extension of the model.

In order to obtain an analytical solution to Eq 44, a linearising simplification to the expression for seabed shear stress is made. Substituting Eq 41 into Eq 42 gives,

$$\tau = \rho\, C_{fc}\, (U_m \exp(i[\omega t-\varphi]) + U_o)\left|U_m \cos(\omega t-\varphi) + U_o\right| \tag{45}$$

It is assumed that the maximum value of the modulus holds at all times. τ will therefore be well predicted close to its maximum and less well away from it, although the most important effects of friction on current velocities occur around the maximum. The expression used for τ is therefore,

$$\tau = \rho\, C_{fc}\, (U_m \exp(i[\omega t-\varphi]) + U_o)\, (U_m + \left|U_o\right|) \tag{46}$$

The solution to the momentum balance equation is found by substituting Eqs 37, 41 and 46 into Eq 44, and equating time-independent and time-dependent parts,

$$\rho\, C_{fc}\, U_o(U_m + \left|U_o\right|) = F - \rho g S_o \tag{47}$$

and $$gS_m \exp(i[\omega t-\Theta]) + i\omega U_m \exp(i[\omega t-\varphi]) + \frac{C_{fc} U_m (U_m+\left|U_o\right|)\exp(i[\omega t-\varphi])}{h} = 0 \tag{48}$$

Equating the amplitude and phase parts of Eq 48 yields,

$$g^2 S_m^2 = \omega^2 U_m^2 + \left(\frac{C_{fc} U_m (U_m + |U_o|)}{h}\right)^2 \tag{49}$$

and $$\varphi = \Theta + \tan^{-1}\left[\frac{-\omega h}{-C_{fc}(U_m + |U_o|)}\right] \tag{50}$$

Eq 47 and 49 represent coupled expressions for the two unknowns U_m and U_o. φ is found from Eq 50 once U_m and U_o are known. An efficient scheme for solving these equations is described in Southgate (1988).

The solutions to the problems of steady currents only, and oscillatory currents only, are special cases of Eqs 47, 49 and 50. Putting U_m to zero in Eq 47 gives the solution for steady currents only,

$$U_o = \kappa \left(\frac{|F - \rho h g S_o|}{\rho C_{fc}}\right)^{1/2} \qquad \text{(Steady currents only)} \tag{51}$$

in which κ is the sign of $F-\rho h g S_o$. For oscillatory currents only, U_o is set to zero in Eqs 49 and 50. Eq 49 then becomes a quadratic in U_m^2 with solution,

$$U_m = \frac{1}{\sqrt{2}} \left(\frac{\omega h}{C_{fc}}\right) \left[\left(1 + \frac{4 g^2 S_m^2 C_{fc}^2}{h^2 \omega^4}\right)^{1/2} - 1\right]^{1/2} \text{(Oscillatory currents only)} \tag{52}$$

This equation simplifies further if the balancing forces are either inertia dominated ($2gS_m C_{fc}/h\omega^2 \ll 1$) or friction dominated ($2gS_m C_{fc}/h\omega^2 \gg 1$),

$$U_m = \frac{gS_m}{\omega} \quad \text{(Oscillatory currents only, Inertia dominated)} \qquad (53)$$

$$U_m = \left(\frac{hgS_m}{C_{fc}}\right)^{1/2} \quad \text{(Oscillatory currents only, Friction dominated)} \qquad (54)$$

A comparison of predicted tidal current velocities with field data is given in Section 5.

4 COMPARISON WITH LABORATORY DATA

In order to test the model, comparisons have been made with laboratory measurements. Unfortunately no suitable laboratory measurements have been carried out in which both tidal-oscillatory and steady currents, as well as waves, are simulated. However, a number of experimental investigations have been reported in which waves and wave-induced currents have been measured in a laboratory simulation of a straight beach with parallel depth contours. The omission of tidal-oscillatory currents means that the full scope of the computational model would not be tested in such a comparison, but it would provide a useful first stage in the verification of the model.

The laboratory measurements selected for this comparsion were those by Visser (1982, 1984a and 1984b) who measured wave heights, set-up and wave-induced longshore currents, with monochromatic wave input. A feature of Visser's experiments was the careful use of a distribution system to prevent end effects from contaminating the longshore currents. Full details of the experimental arrangements are given in Visser (1982). Other researchers such as Yoo and O'Connor (1987), Pechon (1987) and Bonneton and

Gaillard (1985) have also used Visser's measurements for comparison with their own computational models.

Seven tests were carried out by Visser, three with a smooth concrete 1 in 10 beach slope, three with a 1 in 20 slope, and one with a roughened 1 in 20 slope using bonded gravel. Each test was carried out with different incident wave conditions (Table 1). These tests were reproduced in the computational model using a grid spacing of 0.1m for the 1 in 10 slope, and 0.2m for the 1 in 20 slope. A range of tests was carried out to determine optimum values of the three empirical parameters used by the model, the bed roughness k_s (which determines the wave and current friction factors), the breaking dissipation factor λ, and the breaker height factor a'. These values are shown in Table 2.

In his numerical model, Visser used best-fit values for k_s of 1.2mm and 1.5mm (depending on other model assumptions) for the 1 in 10 slope, 0.4mm and 0.8mm for the 1 in 20 slope, and 5mm and 15mm for the roughened 1 in 20 slope. The results of the first of the seven comparisons (for the 1 in 10 slope) are given in Fig 2 showing respectively longshore current velocities, set-up and wave heights. Similar conclusions can be drawn from results from the other six tests; these are presented in the research report, Southgate (1988).

An important finding from Visser's experiments was that the wave set-up and wave-induced longshore currents did not start their strong increase at the breaker line (where maximum wave height occurs, immediately before breaking) but at the plunge line (where the plunging breaker strikes the still water). There is a significant distance between these two lines, of about ¼ to ½ of

the entire width of the surf zone, during which the wave height decreases rapidly as the crest curls over, but the water motion remains essentially irrotational and the excess momentum flux is not released from the waves.

The method used in the computational model to deal with this problem is to "tune" the breaking process so that waves appear to break either at the breaker point or the plunge point. The idea is that if wave quantities are of principal interest in a particular application the model would be tuned to the breaker line, whereas if radiation-stress-related quantities (i.e. surf zone processes driven by radiation stress forces) are of principal interest the model would be tuned to the plunge line. It was found that the onset of breaking could be made to occur nearer to the shoreline by increasing the value of a' in the breaker height criterion, Eq 13. The model results presented in Fig 2 were tuned to the plunge line using a value of a'=1.18, larger than the usually used value of 0.78 for tuning to the breaker line. The model tests were then repeated with a'=0.78 (Fig 3). It can be seen that in these latter tests the maximum longshore current and the minimum set-up occur too far seawards in the model, but that the wave heights are much better predicted, especially in the decay landwards of the breaker line.

The tests described so far have used a simulation of the breaking of random waves (although in all other respects the waves have been treated as monochromatic). Further model tests were performed, treating the breaking process as applying to monochromatic waves. Results from these runs are shown in Fig 4 and they indicate that the wave set-up and the longshore current velocity are poorly predicted, with the longshore current velocity sharply decreasing seawards of the plunge line. It can be seen from Fig 4C,

however, that there is an improvement to the prediction of wave heights around the maximum, as would be expected since the experimental waves were monochromatic. However, the maximum is still underpredicted, and this is probably due to the absence of any modelling of non-linear processes which cause a greater peaking of wave height just before breaking. Some idea of the relative importance of these contributions (ie random versus monochromatic wave breaking, and absence of non-linearities) to the error in wave height at the breaker line can be seen by comparing results from the present model with those from two models used by Pechon (1987). These models respectively incorporated linear and non-linear (Serre theory) monochromatic waves (see Table 3).

Another feature to be commented on is the method of modelling the wave-induced longshore currents. For monochromatic waves, lateral diffusion due to turbulence within the surf zone plays an important part in determining the cross-shore distribution of longshore currents. Without the effects of lateral diffusion, a sharp cut-off at the plunge line is obtained (Fig 4A). Inclusion of lateral diffusion gives a significant longshore current seawards of the plunge line. For random waves, however, the effects of lateral diffusion are far less noticeable since a similar smoothing of the longshore current distribution is caused by the randomness in the locations of the breaker and plunge lines. Researchers such as Battjes (1972) and Thornton and Guza (1986) have concluded that computational models which employ a random wave breaking formulation with no explicit modelling of lateral diffusion will provide sufficiently accurate predictions of wave-induced longshore currents under random waves for practical purposes. The good agreement between experiment and model predictions in the present study, using realistic and consistent values for the empirically-determined

variables, tends to bear out this conclusion. The conclusion is in fact extended further, in the sense that the cross-shore distribution of longshore currents from monochromatic breaking waves can be modelled by a random wave breaking formulation, with waves being regarded as monochromatic in all other respects.

This finding is important for engineering models where computing speed is a prime consideration. It should be emphasized however that the physical mechanism determining the longshore current distribution is one of lateral diffusion, and this should be incorporated in any computational model which aims at a physically comprehensive representation of the surf zone.

5 COMPARISON WITH FIELD DATA

Field data obtained to date have not been entirely suitable for testing the full scope of the model, either through lack of sufficiently comprehensive simultaneous wave and tidal current measurements, or through locations being chosen where tidal currents are weak. In the absence at the present time of a suitable comprehensive field data set, the model has been compared with a small series of tidal current velocity measurements made at a coastal site immediately to the north of Aberdeen Harbour in Scotland (Fig 5).

The coastline north of Aberdeen is long and straight with a regular seabed slope out to deep water, making it a good site at which to test the model. The measurements consisted of float-tracking from five release-points on a shore-normal line north of the harbour (Fig 5). The release-points were sufficiently close to the harbour for the north-flowing tidal currents to be significantly distorted by the harbour and the adjacent headland, Girdle

Ness. Accordingly, measurements were only made on the south-flowing tide, although even for these some distortion occurs due to the presence of the harbour and headland. Three sets of measurements at different states of the tide were made.

The computational model was set up with 41 grid points between deep water and the beach. Since conditions were calm during the field exercise, the model was run to determine tidal currents only, with no waves. Tidal currents were predicted at twenty stages during a semi-diurnal tidal cycle for each release-point. The tidal quantities needed for input to the model were deduced from information on tidal elevations and phases published in Tide Tables. Sediment samples indicated a fine to medium sand, and k_s was set to a value appropriate to a ripple height for this type of sand, of 0.016m. In this comparison, the model was used as a predictive tool; no adjustments were made to the input parameters to obtain a best fit.

The comparison between the measured longshore tidal current velocities and the model predictions is shown in Fig 6. The full lines represent the model tidal curves, and the large symbols represent the measured current velocities. It can be seen that two of the three sets of measurements (at approximately HW-5½hrs and HW-½hr) show good agreement with the model predictions, particularly in determining the relative phases of the current velocities at the different release-points. The importance of tidal inertia is seen in the measured currents at HW-5½hrs, when the currents have turned south-going at all the shallower depths but at 16m the current is still north-going. At HW-½hr the current at 1m depth has turned north-going but at the deeper points it is still south-going. The third set of measurements, close to the maximum predicted southerly currents, shows that

the model considerably over-predicts at the smaller depths. It is probable that these strong southerly currents were deflected seawards by being close to the harbour, and charts of the float paths showed that this was so. The agreement between the model predictions and measurements appears promising, but a proper validation requires a comparison with data from a comprehensive field exercise including the interaction of waves and tides.

6 CONCLUSIONS

A computational model for predicting wave and current conditions in nearshore regions, under the 1-D approximation, has been presented. Longshore tidal currents and wave-induced currents are included, with full interaction between the waves and the two types of current. The model is designed to be used as an engineering tool for the prediction of long-term hydrodynamic and morphological processes, and is capable of analysing many thousands of input wave and tidal values. As a consequence it is possible to put beach and nearshore processes into a statistical context. This is often of more value to a coastal engineer than a very detailed study of hydrodynamics or sediment motion under a limited range of wave and tidal conditions.

Comparison with experimental measurements of wave heights, set-up of the still water level, and wave-induced longshore currents have indicated good agreement. The model needs to be tuned to the breaker line for the prediction of wave heights, and to the plunge line for radiation-stress-related quantities. The use of a random wave breaking formulation has been shown to give sufficiently accurate predictions for practical purposes of wave-induced longshore currents, without any explicit modelling of lateral

diffusion. The model has also been compared with field measurements of tidal currents.

The separate comparisons of wave (and wave-induced) quantities and tidal quantities have yielded promising results, but further research is necessary to investigate the performance of the model in situations where both processes interact. Results from the model run interactively have indicated significant reduction in both wave-induced and tidal longshore currents compared with the non-interactive case (Southgate, 1987). The verification of these effects ideally requires a field exercise at a straight-coast location with strong tidal currents, and with simultaneous and comprehensive measurements of wave and current conditions within and outside the surf zone.

ACKNOWLEDGEMENTS

The author would like to thank his colleague R L Soulsby for his many helpful discussions in the course of this work. Prof B A O'Connor and Dr D Yoo of the Department of Civil Engineering at Liverpool University are thanked for discussions on their wave-current friction model. Financial support for this work was provided by the UK Ministry of Agriculture, Fisheries and Food.

LIST OF SYMBOLS

a	Breaking parameter Eq 13
a'	Empirical breaking factor
b	Breaking parameter Eq 14

C_{fc}	Current friction factor
C_{fw}	Wave friction factor
c_{ga}	Absolute wave group velocity Eq 5
c_{gr}	Relative wave group velocity Eq 4
c_r	Relative wave celerity Eq 3
D_b	Spatial rate of dissipation of wave energy flux due to breaking
D_f	Spatial rate of dissipation of wave energy flux due to seabed friction
E	Wave energy per unit sea area Eq 9
f(Q)	Defined by Eq 19
F	Driving force from wave radiation stresses Eq 33
g	Acceleration due to gravity
h	Water depth
H	Wave height
H_b	Wave height at the breaker point
H_{rms}	Root-mean-square wave height in the Rayleigh distribution with truncation
i	$\sqrt{-1}$
k	Wavenumber Eq 1
k_s	Seabed roughness length
K_d	Doppler coefficient Eq 24
K_r	Refraction coefficient Eq 23
K_s	Shoaling coefficient Eq 22
m	Seabed slope
P(H)	Rayleigh probability distribution of wave heights Eq 15
Q	Probability of occurrence of a broken wave Eq 16
S	Longshore water surface slope due to longshore tidal variations Eq 37
S_m	Maximum value of oscillatory component of S

S_o	Steady component of S
S_{xy}	Wave radiation stress in the longshore direction
S_{yy}	Wave radiation stress in the onshore direction
t	Time
U	Longshore current velocity Eq 41
U_m	Maximum value of oscillatory component of U
U_o	Steady component of U
V_o	Maximum water particle velocity at seabed Eq 11
x	Longshore co-ordinate
y	Onshore co-ordinate
α	Angle between wave orthogonal and onshore direction
β	Wave energy dissipation factor Eq 25
δ	Angle between longshore current and onshore direction
ϵ	Wave energy dissipation factor Eq 32
ζ	Surface elevation above mean sea level Eq 35
ζ_m	Maximum value of ζ
η	Wave set-up
Θ	Phase of oscillatory component of S
κ	Sign of $F-\rho hgS_o$, Eq 51
λ	Empirical breaking factor
μ	Angle between wave ray and onshore direction Eq 6
ρ	Water density
τ	Shear stress at the seabed Eq 42
ϕ	Phase of oscillatory component of ζ
φ	Phase of oscillatory component of U
ω	Tidal angular frequency
ω_a	Absolute wave angular frequency
ω_r	Relative wave angular frequency Eq 2

Subscripts

i	Denotes present grid point
o	Denotes previous grid point (further offshore)

REFERENCES

Abernethy C L and Gilbert G. 1975, "Refraction of wave spectra", Report IT 117, Hydraulics Research Station.

Battjes J A. 1972, "Set-up due to irregular waves", Proc 13th International Conference on Coastal Engineering, ASCE, pp 1993-2004.

Battjes J A and Janssen J P F M. 1978, "Energy loss and set-up due to breaking of random waves", Proc 16th International Conference on Coastal Engineering, ASCE, Hamburg, pp569-587.

Bijker E W. 1966, "The increase of bed shear in a current due to wave motion", Proc. 10th International Conference on Coastal Engineering, ASCE, Vol 1, pp 746-765.

Bonneton M and Gaillard P. 1985, "Numerical calculation of wave-induced currents", IAHR 21st Congress, Melbourne, Australia.

Booij N. 1981, "Gravity waves on water with non-uniform depth and current", Report No 81-1, Department of Civil Engineering, Delft University of Technology.

Booij N, Holthuijsen L H and Herbers T H C. 1985, "A numerical model for wave boundary conditions in port design", International Conference on Numerical and Hydraulic Modelling of Ports and Harbours, Birmingham, England.

Brampton A H and Motyka J M. 1987, "Recent examples of mathematical models of UK beaches", ASCE Speciality Conference on Coastal Sediments, New Orleans, USA.

Christoffersen J B and Jonsson I G. 1980, "A note on wave action conservation in a dissipative current wave motion", Applied Ocean Research, Vol 2, pp 179-182.

Christoffersen J B and Jonsson I G. 1985, "Bed friction and dissipation in a combined current and wave motion", Ocean Engineering, Vol 2, pp 387-423.

Dalrymple R A, Kirby J T and Hwang P A. 1984, "Wave diffraction due to areas of energy dissipation", Journal of Waterway, Port Coastal and Ocean Engineering, ASCE, Vol 110, No 1.

Hubertz J M. 1984, "Modelling of nearshore wave driven currents", 17th International Conference on Coastal Engineering, ASCE, Houston, USA.

Jonsson I G and Christoffersen J. 1984, "Current depth refraction of regular waves", 17th International Conference on Coastal Engineering, ASCE, Houston, USA.

Kirby J T. 1984, "A note on linear surface wave-current interaction over slowly varying topography", Journal of Geophysical Research, Vol 89, No C1, pp 745-747.

Komar P D and Inman D L. 1970, "Longshore sand transport on beaches", Journal of Geophysical Research, Vol 75, No 30, pp 5914-5927.

Longuet-Higgins M S. 1970, "Longshore currents generated by obliquely incident sea waves 1", Journal of Geophysical Research, Vol 75, No 33.

O'Connor B A and Yoo D. 1988, "Mean bed friction of combined wave-current flow", Coastal Engineering, Vol 12, No 1.

Ozasa H and Brampton A H. 1980, "Mathematical modelling of beaches backed by seawalls", Coastal Engineering, Vol 4, No 1.

Pechon P. 1987, "Modelling of longshore currents with a non-linear wave theory", ASCE Speciality Conference on Coastal Hydrodynamics, Delaware, USA.

Price W A, Tomlinson K W and Willis D H. 1972, "Predicting changes in the plan shapes of beaches", 13th International Conference on Coastal Engineering.

Shore Protection Manual. US Army Coastal Engineering Research Centre, US Govt Printing Office. Revised periodically.

Skovgaard O, Jonsson I G and Bertelsen J A. 1975, "Computation of wave heights due to refraction and friction", Journal of Waterways, Harbours and Coastal Engineering Division, ASCE, vol 101, pp 15-32.

Southgate H N. 1987, "A one-dimensional model of wave-current interaction", ASCE Speciality Conference on Coastal Hydrodynamics, Delaware, USA.

Southgate H N. 1988, "The nearshore profile model", Report SR 157, Hydraulics Research Ltd.

Stive M J F and De Vriend H J. 1987, "Quasi-3D nearshore current modelling: wave-induced secondary current", ASCE Speciality Conference on Coastal Hydrodynamics, Delaware, USA.

Stive M J F and Wind H G. 1982, "A study of radiation stress and set-up in the nearshore region", Coastal Engineering, Vol 6, pp1-25.

Thornton E B and Guza R T. 1986, "Surfzone longshore currents and random waves: field data and models", Journal of Physical Oceanography, Vol 16, No 7, pp 1165-1178.

Townend I M and Savell I A. 1984, "The application of ray methods to wave refraction studies", Offshore and Coastal Modelling, 7th POLYMODEL Conference, Sunderland Polytechnic.

Treloar P D. 1986, "Spectral wave refraction under the influence of depth and current", Coastal Engineering, Vol 9, pp 439-452.

Visser P J. 1982, "The proper longshore current in a wave basin", Report No 82-1, Department of Civil Engineering, Delft University of Technology.

Visser P J. 1984a, "A mathematical model of the uniform longshore currents and the comparison with laboratory data", Report No 84-2, Department of Civil Engineering, Delft University of Technology.

Visser P J. 1984b, "Uniform longshore current measurements and calculations", 19th International Conference on Coastal Engineering, ASCE, Houston, USA.

Weggel J R. 1972, "Maximum breaker height", Journal of Waterways, Harbours and Coastal Engineering Division, ASCE, Vol 98.

Wind H G and Vreugdenhil C B. 1986, "Rip-current generation near structures", Journal of Fluid Mechanics, Vol 171, pp 459-476.

Yoo D and O'Connor B A. 1986, "Mathematical modelling of wave-induced nearshore circulations", 20th International Conference on Coastal Engineering, ASCE, Taipei, Taiwan.

Yoo D and O'Connor B A. 1987, "Bed friction model of wave-current interacted flow", ASCE Speciality Conference on Coastal Hydrodynamics, Delaware, USA.

TABLE 1 Beach and Wave values used in Visser's experiments. P = Plunging, S = Spilling

Exp Number	1	2	3	4	5	6	7
Beach Type	Smooth	Smooth	Smooth	Smooth	Smooth	Smooth	Rough
Beach Slope	0.101	0.101	0.101	0.050	0.050	0.050	0.050
Wave Period(s)	2.01	1.00	1.00	1.02	1.85	0.70	1.02
Offshore Depth(cm)	39.9	39.9	40.1	35.0	34.8	35.0	35.0
Offshore Wave Angle(degr)	31.1	30.5	15.4	15.4	15.4	15.4	15.4
Offshore Wave Height(cm)	7.2	9.5	8.9	7.8	7.1	5.9	7.8
Breaker Line Depth(cm)	10.4	10.9	11.4	11.0	11.6	8.8	12.2
Breaker Line Wave Angle(degr)	20.9	24.0	12.1	12.5	11.5	14.3	12.2
Breaker Line Wave Height(cm)	10.5	10.0	9.7	9.1	10.8	5.8	9.0
Maximum Wave Set-up(cm)	4.20	2.78	2.75	1.64	2.45	1.00	1.64
Breaker Type	P	P	P	P	P	P/S	P

TABLE 2 Best-fit values of empirically-determined parameters

Empirical Parameter	Best-Fit Value in Model		
	1 in 10 Slope	1 in 20 Slope	1 in 20 slope Roughened
k_s	2mm	0.6mm	10mm
λ	1	1	1
a' (tuned to plunge line)	1.18	1.18	1.18
a' (tuned to breaker line)	0.78	0.78	0.78

TABLE 3 Predictions of Wave Height at the Breaker Line by various models for Visser's Experiment One

Computational Model	Wave Height at Breaker Line (Visser Expt One) (cm)	% Difference from Measured Wave Heights
Measurement	10.5	-
Present Model Linear Random Waves	8.7	-17.1%
Present Model Linear Monochromatic Waves	9.7	- 7.6%
Pechon (1987) Linear Monochromatic Waves	9.1	-13.3%
Pechon (1987) Non-Linear Monochromatic Waves	10.8	+ 2.9%

FIGURE CAPTIONS

1. Model geometry of the nearshore region

2. Comparison between computational model and Visser experiments. Test 1, Random wave breaking, a' = 1.18. P and B denote plunge and breaker points.

3. Comparison between computational model and Visser experiments. Test 1, Random wave breaking, a' = 0.78. P and B denote plunge and breaker points.

4. Comparison between computational model and Visser experiments. Test 1, Monochromatic wave breaking, a' = 1.18 for A) and B), a' = 0.78 for C). P and B denote plunge and breaker points.

5. Location of Aberdeen Harbour showing float-release points

6. Comparison of tidal current velocity measurements at Aberdeen with computational model predictions

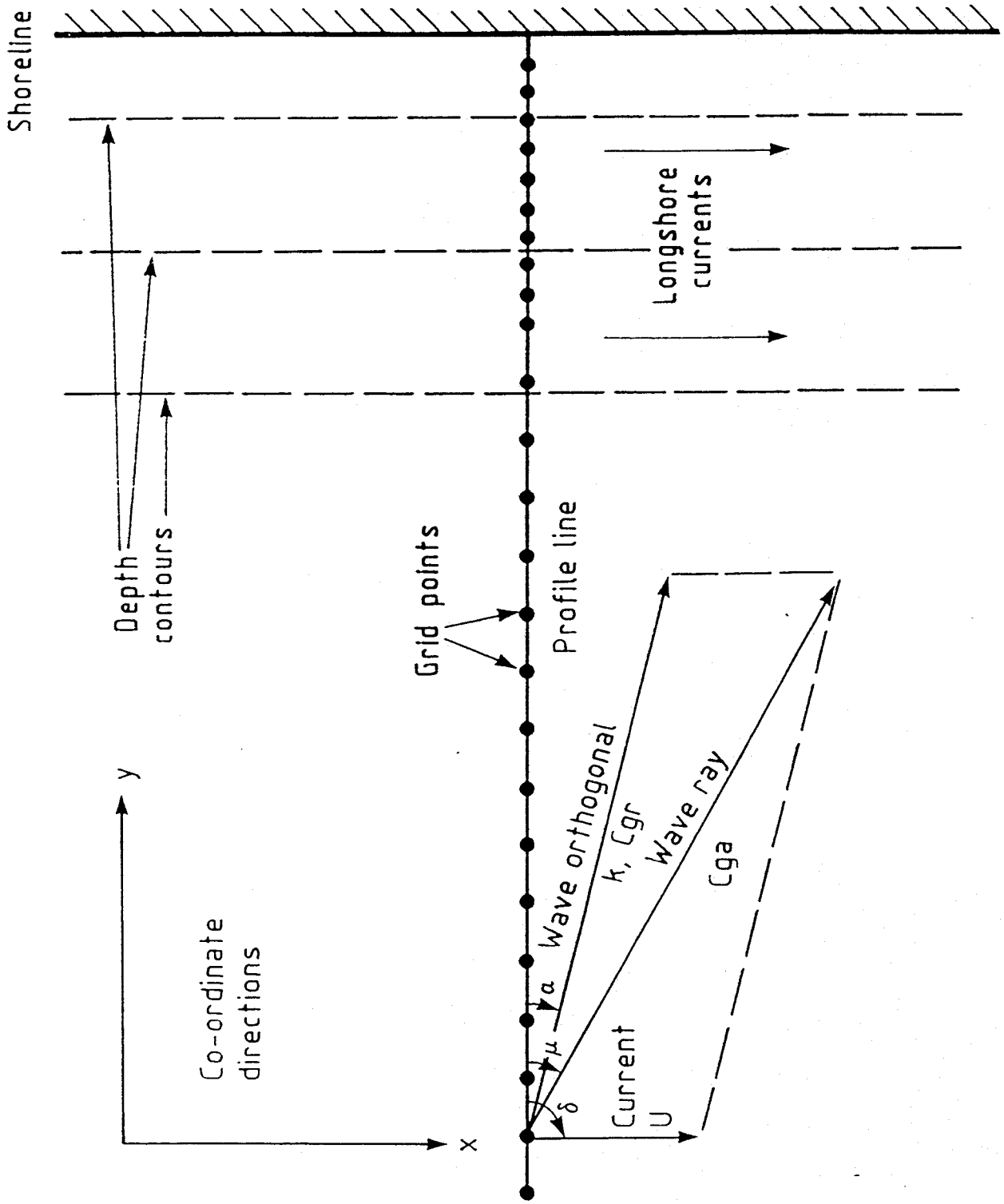

Fig 1 Appx 1 See caption list

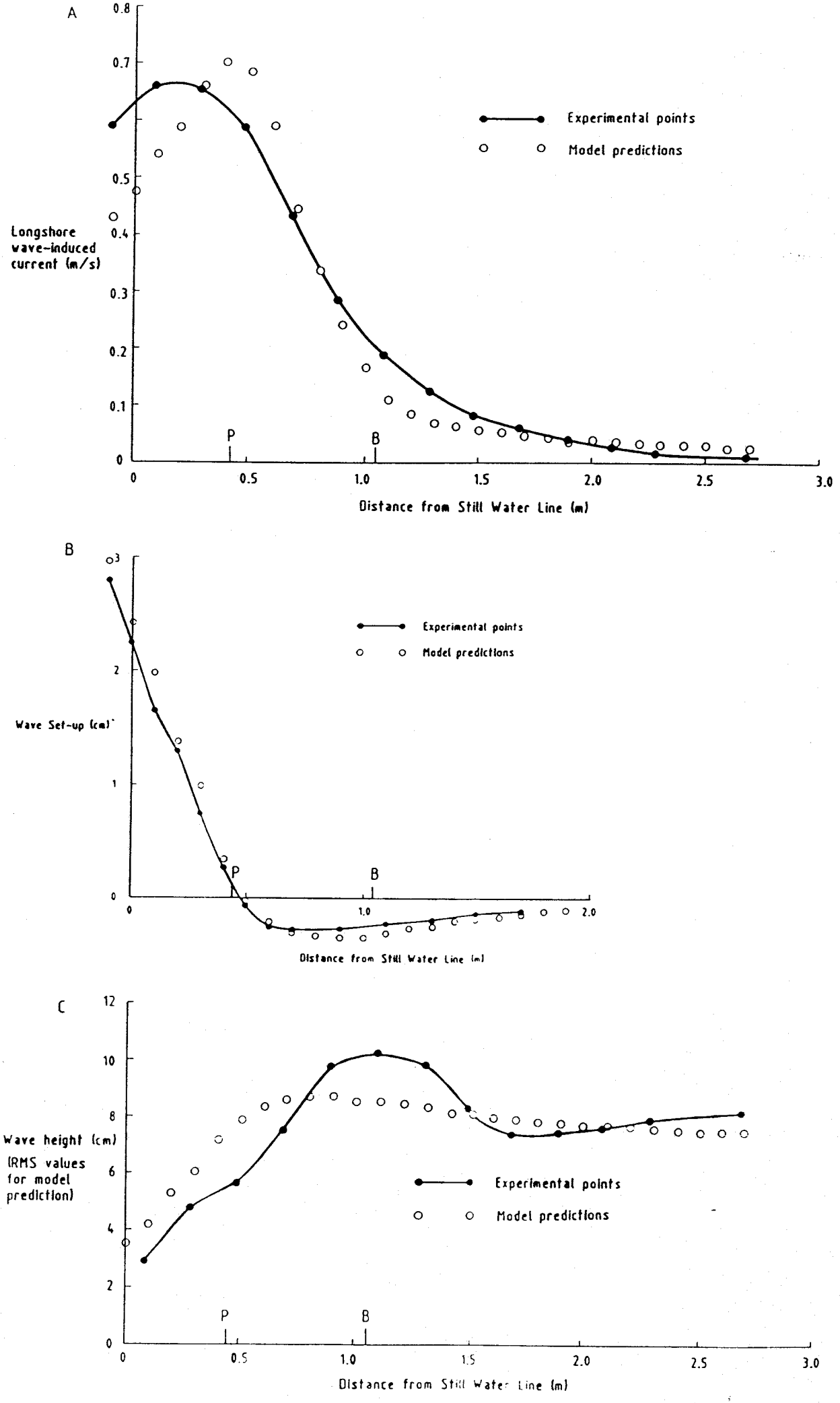

Fig 2 Appx 1 See caption list.

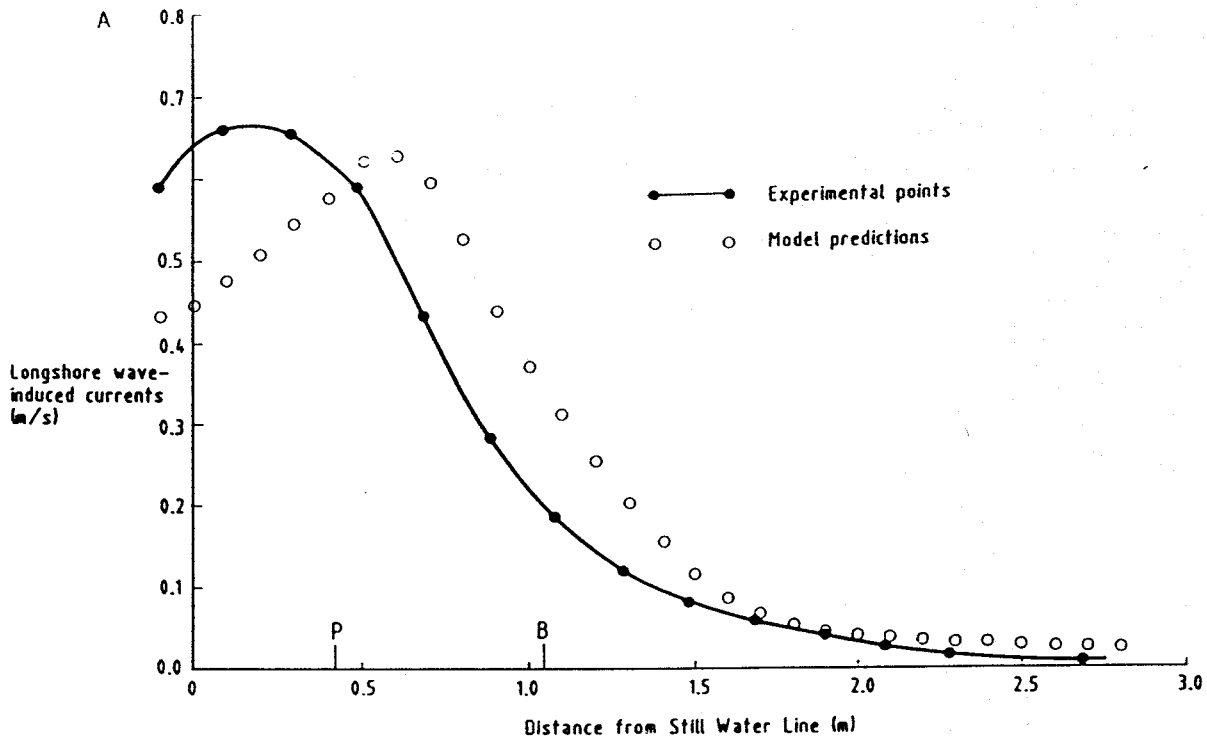

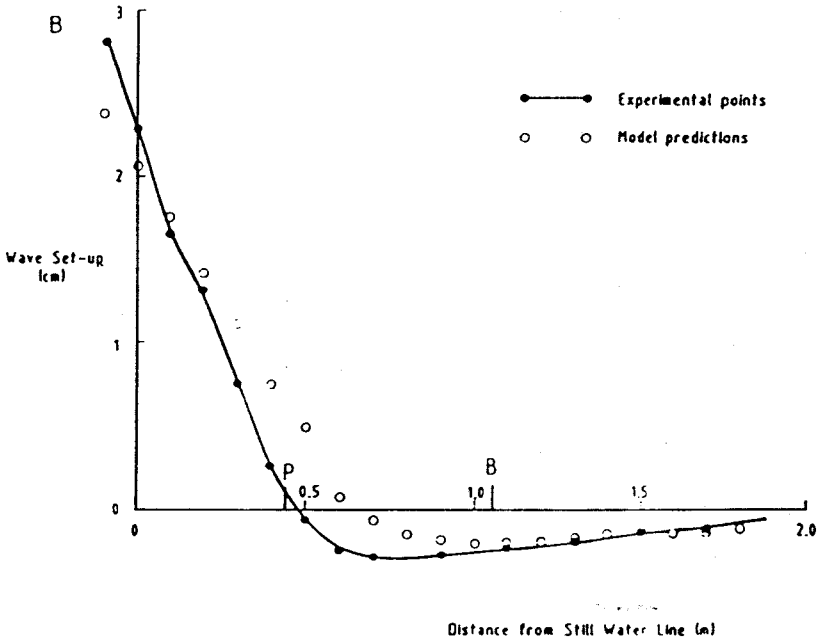

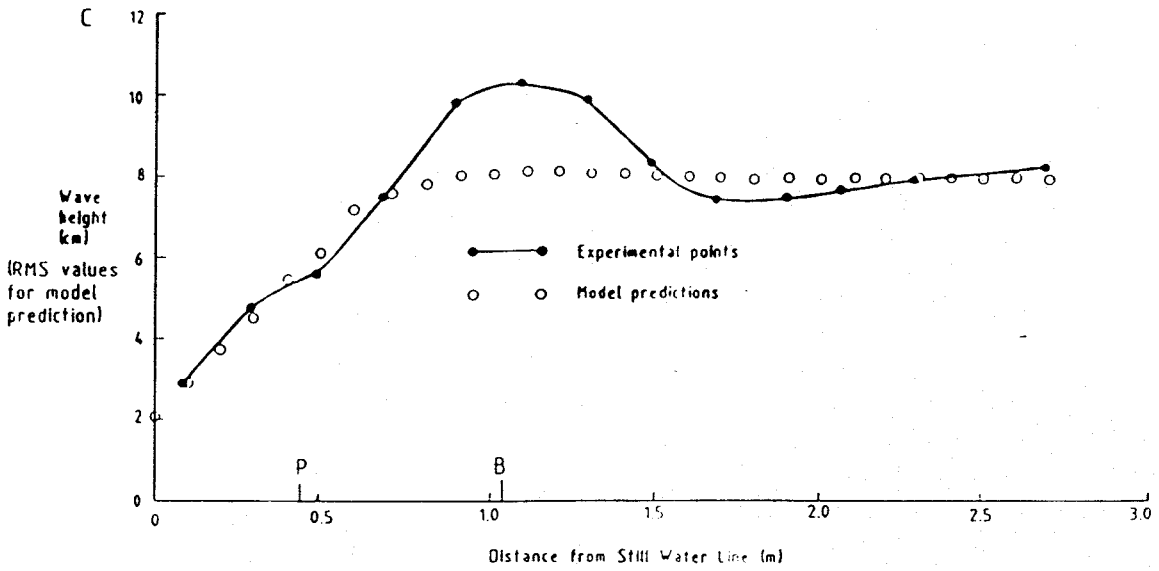

Fig 3 Appx 1 See caption list

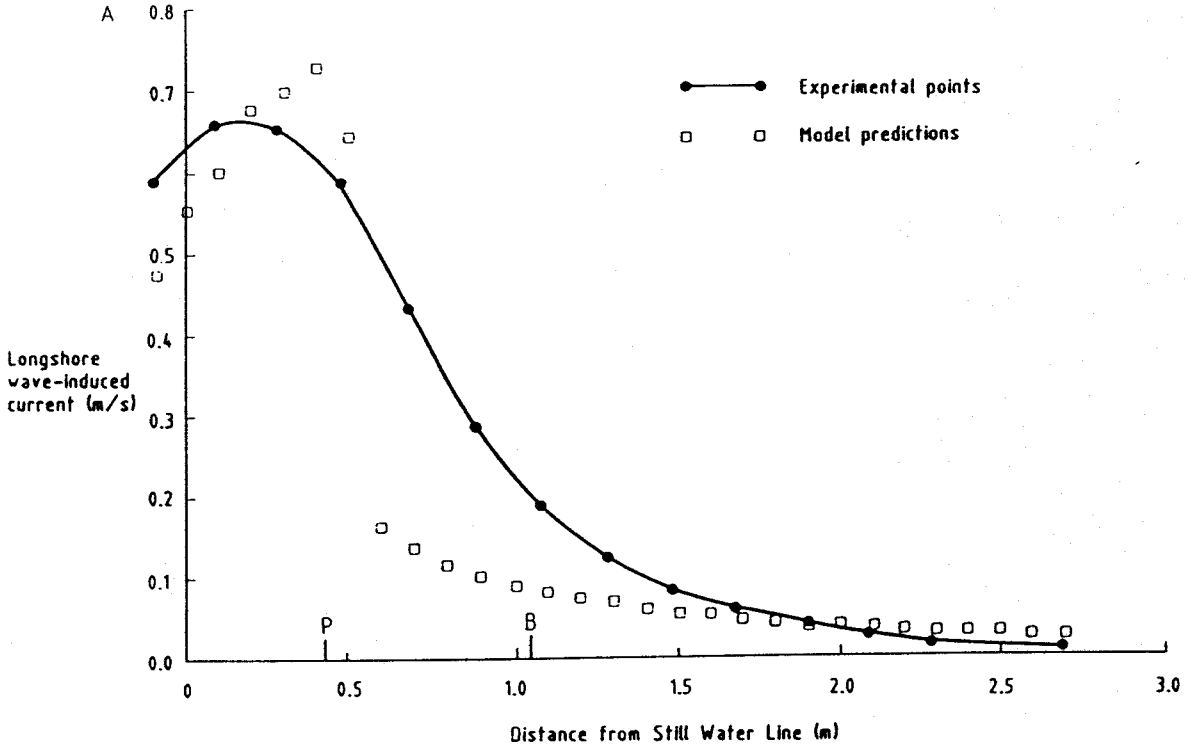

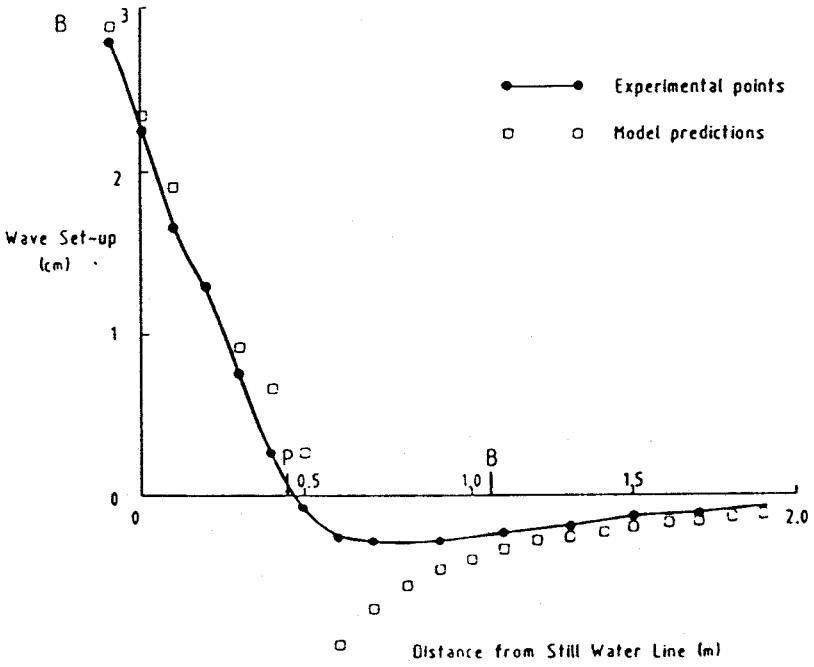

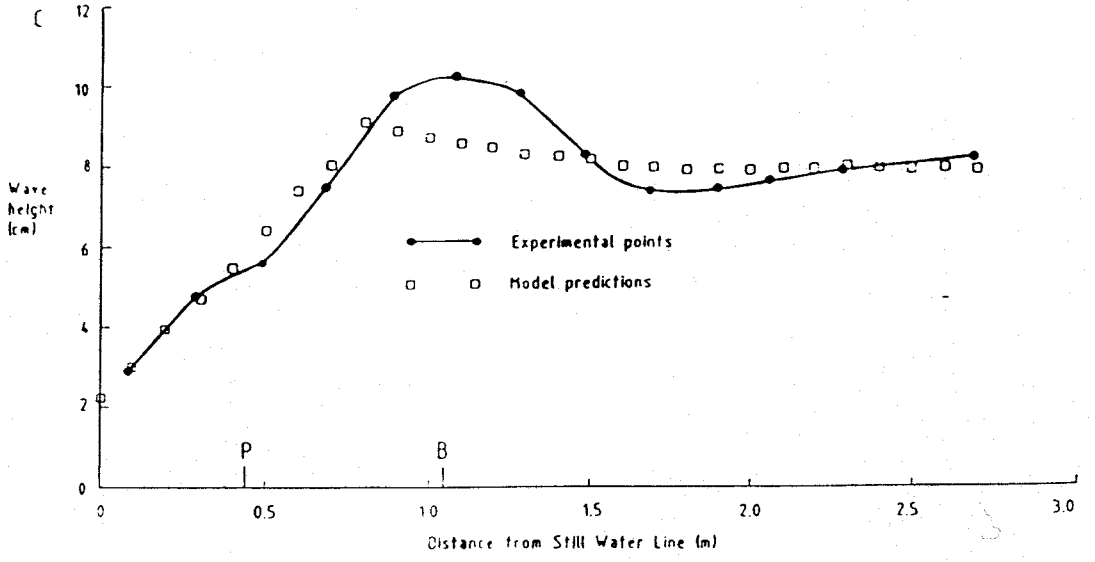

Fig 4 Appx 1 See caption list

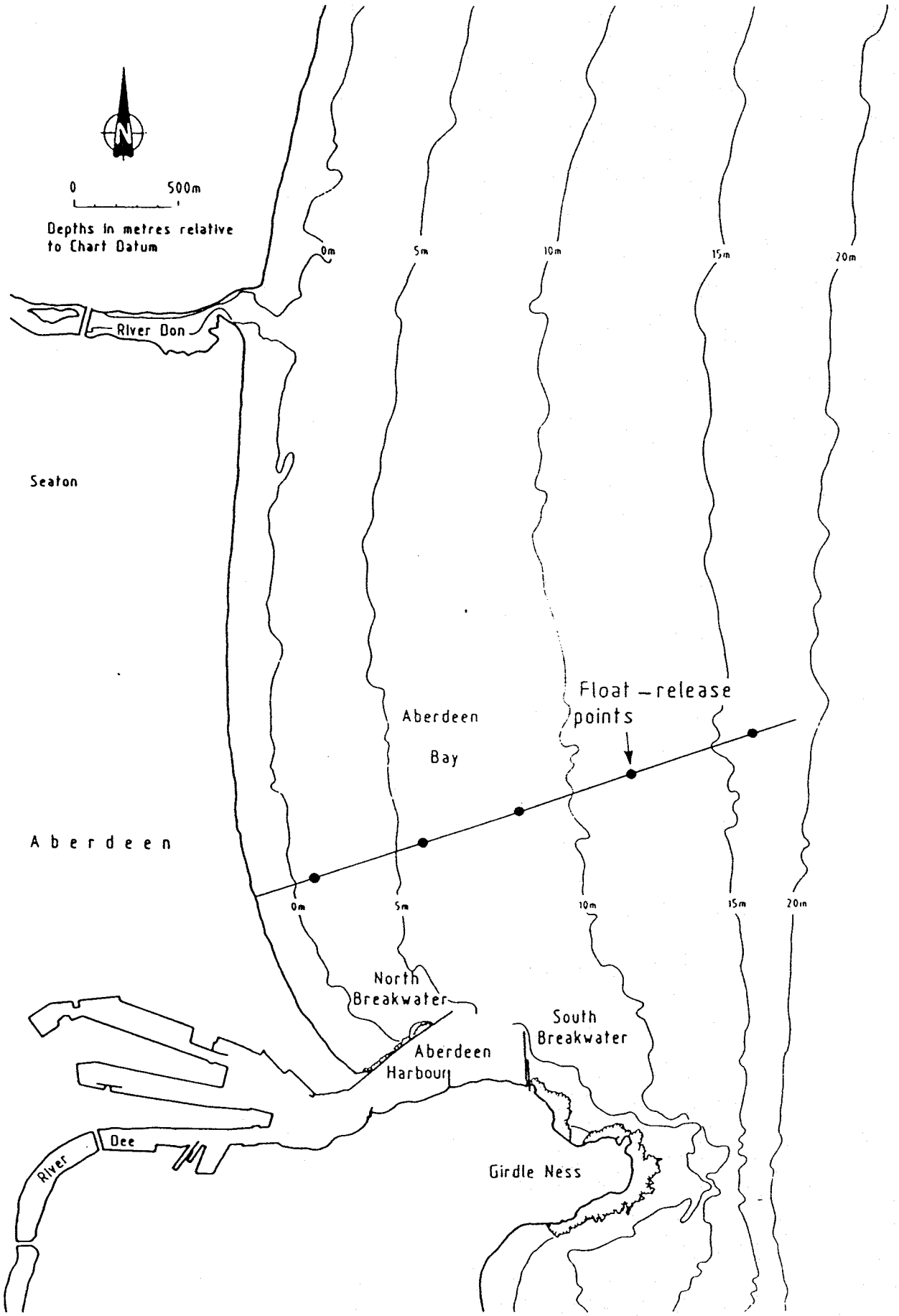

Fig 5 Appx 1 See caption list

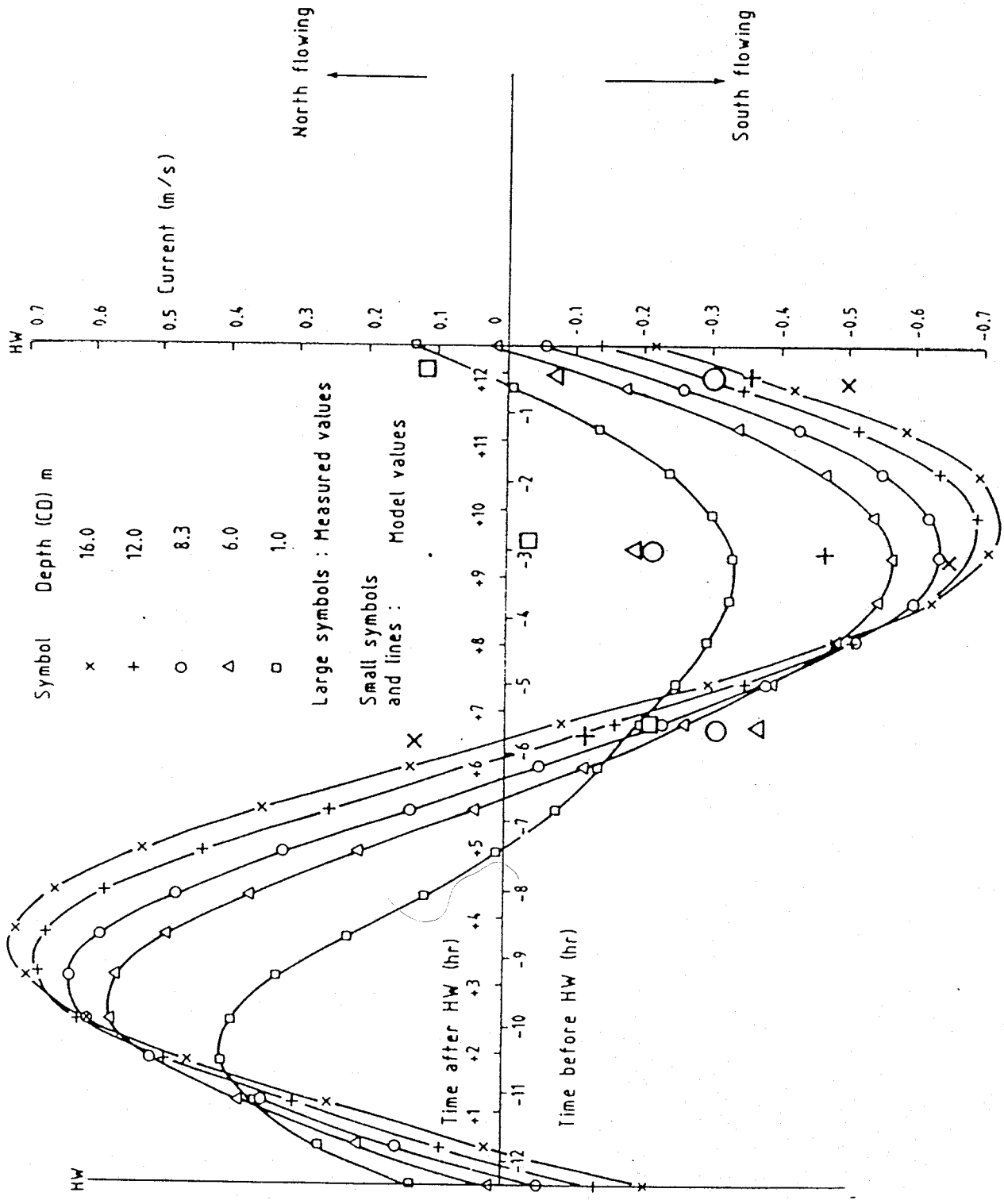

Fig 6 Appx 1 See caption list